Effects of Solution Rheology on Electrospinning of Polystyrene

by

Goki Eda

A Thesis

Submitted to the Faculty

of the

WORCESTER POLYTECHNIC INSTITUTE

In partial fulfillment of the requirements for the

Degree of Master of Science

in

Materials Science and Engineering

April 2006

APPROVED:

Satya Shivkumar, Major Advisor and Professor of Mechanical Engineering

---
Richard D. Sisson, Jr., George F. Fuller Professor of Mechanical Engineering, Director of Manufacturing and Materials Engineering

Abstract

The effects of fundamental solution parameters including polymer molecular weight, concentration and solvent on electrospinning of polystyrene were investigated. Each parameter was found to play a vital role in determining the morphology of beads and fibers. For dilute to semi-dilute solutions, a wide range of bead structures including wrinkled beads, cups, dishes, and toroids were observed when a volatile solvent, tetrahydrofuran, was used. Various rheological regimes where these structures may be obtained were identified. The morphological transition from bead to fiber was characterized by two critical concentrations, C_i and C_f, at which incipient and complete fibers may be observed respectively. These values were determined as a function of molecular weight. A comparison with the models proposed in the literature indicated that solvent evaporation may play an important role in jet stabilization. The fiber diameter and distribution was found to decrease significantly with molecular weight at the critical concentration, C_f. The use of N,N-dimethylformamide, a solvent with relatively high dielectric constant, also resulted in an appreciable reduction in fiber diameter and improved uniformity. The observation of solution jet evolution during the process with high speed camera (2000 frames/s) indicated that solvents have a significant influence on the jet breakdown behavior. Two types of behavior were identified based on the extent of extensional flow, bending instability, and the number of secondary jets. Solvents with high dielectric constant were found to induce extensive bending instability, which resulted in extremely fine microstructures of electrospun polymer.

Acknowledgements

I would like to express my sincere gratitude to Prof. Shivkumar, my thesis advisor, for his patient guidance, thoughtful advices, and constant encouragement. He has made my experience at WPI invaluable. I would also like to thank the faculty and staff in Materials Science and Engineering program for providing me all the help and also the opportunity to work as a Teaching Assistant. I am certain that I learned a tremendous amount from this experience. My thanks definitely go to my roommates, Xiaoshu Dai, Arnaud Gateaud, and Pierre-Alexandre Legait for sharing time, thoughts, and laughs. Life in Worcester would've never been the same.

I would also like to thank my family for all the support and love.

I would also like to thank the Ministry of Education, Culture, Sports, Science and Technology of Japan for financial support.

Table of contents

0. Introduction

Electrospinning is a process in which electrostatic forces are utilized to produce polymer fibers with micro- to nanometer diameters. The process has long been known since 1934 when it was first patented [1]. The versatility and the ease of process have made electrospinning a popular research topic in the last decade. Recent study has shown that electrospun polymer fiber may be as small as few nanometers [2]. Considering that a typical polymer molecule has a diameter of a few tenths of a nanometer, it can easily be imagined that a significant draw ratio is achieved by electrospinning. A wide range of applications of electrospun fibers include sensors, filtration, protective clothing, wound dressing, drug delivery, tissue scaffolds, etc.

Despite the high potential, the industrial significance of electrospinning is limited due to the low throughput of the process, inconsistent molecular orientation, and large diameter distribution of fibers. A large amount of research effort has been put into determining the fabrication parameters that control the structure and properties of electrospun polymers. Most investigations related to electrospinning of polymers attempt to study the effect of fabrication parameters on one or more of the following: (1) the formation of fundamental structures i.e. beads, beaded fibers, bead-free fibers, (2) their shapes and surface morphology, (3) their size and distribution, and (4) their mechanical, optical, electrical, and biological properties. Although a large number of process parameters have been examined to date, the effect of some of the fundamental parameters have not been thoroughly understood. For instance, knowledge of the influence of molecular weight on the aforementioned features, while recognized as significant, is

limited. In this thesis, the effect of some of the fundamental solution parameters including polymer molecular weight, concentration and solvent properties on the morphology of electrospun polystyrene is examined.

This thesis is presented as a compilation of three journal papers. The following three chapters correspond to each paper:

1. Bead structure variations during electrospinning of polystyrene
2. Bead-to-fiber transition in electrospun polystyrene
3. Solvent effects on jet evolution during electrospinning of semi-dilute polystyrene solution

Different aspects of electrospinning as a function of solution rheology are discussed in each chapter.

Reference

[1] Formhals, A. US Patent 1975504, 1934.
[2] S-H Tan, R. Inai, M. Kotaki, S. Ramakrishna, Polymer 46 (2005) 6128–6134.

Chapter 1

Bead Structure Variations during Electrospinning of Polystyrene

Paper accepted for publication in *Journal of Materials Science*, 2006

Paper accepted for publication in *Journal of Materials Science*, 2006

Bead Structure Variations during Electrospinning of Polystyrene

Goki Eda and Satya Shivkumar*

Materials Science and Engineering Program,
Department of Mechanical Engineering,
Worcester Polytechnic Institute,
100 Institute Road,
Worcester, MA 01609

Abstract

Polystyrene solutions with molecular weights between 19,300 and 1,877,000 g/mol were electrospun with tetrahydofuran as the solvent in the dilute to semi-dilute concentration regime. Various morphologies including wrinkled beads, cups, dishes, and toroids were obtained depending on molecular weight and concentration. Wrinkled beads were generally observed at concentrations near the entanglement concentration. Other types of beads were observed at lower concentrations.

Keywords: Electrospinning; Polystyrene; Molecular Weight

**Tel.:* +1 508 831 5048; *fax:* +1 508 831 5178
E-mail address: shivkuma@wpi.edu

Introduction

One of the attractive features of electrospinning is the capability to produce a wide range of fiber morphologies by controlling various material and process parameters. Other than the typically observed cylindrical fibers, flat, wrinkled, and porous fibers have been reported to date for different polymer-solvent systems [1,2]. Koombhongse et al. [1] suggest that the morphology of the fiber obtained is determined by a complex interaction between fluid flow, electrical forces, and solvent evaporation. During the solidification of the jet, a thin skin of solid polymer can form on the surface, especially if a highly volatile solvent is used. This skin can subsequently collapse and lead to wrinkled and flat fibers. The formation of sub-micron pores on electrospun fibers is another interesting phenomenon, which has attracted attention [2,3]. Reports have shown that humidity, molecular weight and solvent properties play an important role in pore formation. A recent study by Liu et al. [4] indicates that droplets of solution produced by electrospinning can also undergo skin formation and collapse, thereby developing interesting bead shapes and surface morphologies. A variety of bead morphologies including porous beads, microscopic ladles and cups can be produced by using different solvents. Although these results confirmed the significance of solvent evaporation rate and solution viscosity on bead morphology, the effect of molecular weight on attainable bead structures has not yet been explored. The ability to control the bead structures in terms of this fundamental parameter may be important in many industrial polymers for diverse applications including aerosols, surface coatings, membranes, chromatography standards and drug delivery systems. The purpose of this contribution is to examine the

cumulative effects of polymer molecular weight and solution concentration on the bead structure in electrospun polystyrene. The structures that may be produced with dilute solutions before the emergence of stable fiber structures are explored.

Experimental Procedure

Linear polystyrene with various weight average molecular weights (M_w) having a polydispersity index of about 1 were obtained from Scientific Polymer Products, Ontario, NY. Appropriate amounts of the polymer were dissolved in tetrahydrofuran, THF, (Aldrich, reagent grade) to obtain solutions of the desired concentration. Depending on M_w, the solution concentrations were varied between 0.11 and 41.8 wt%, as shown in Table 1. The polymer solution was aspirated into a 1 mL syringe equipped with an 18 gauge needle (inner diameter = 0.84 mm, 51 mm long). The syringe was placed horizontally on a syringe pump (EW-74900-00, Cole-Parmer), which was calibrated to achieve a flow rate of 3 mL/hr. A potential of 10 kV and a tip-to-collector distance of 10 cm was used for all the experiments. The electrospinning apparatus was enclosed in a plexiglass chamber, which was vented during the process in order to control solvent evaporation. All experiments were conducted at room temperature and at a relative humidity between 20 and 30%. The electrospun polymer was sputter-coated with gold-palladium and was examined with a scanning electron microscope (JSM-840).

Results and Discussion

Polymer chain entanglements play a vital role in determining the structure in the electrospun polymer. A bead dominant morphology is generally observed when a minimum degree of chain entanglements is not present [5,6]. One of the approaches to predict the degree of entanglement is to define two critical concentrations C^* and C_e [6]. A polymer molecule in a solution may assume a conformation that is confined in a volume known as the hydrodynamic volume. In a dilute solution, the molecules within this volume are dispersed in the solvent without appreciable interactions. The limiting concentration for dilute solutions, C^*, corresponds to the solution concentration where the hydrodynamic volumes begin to overlap. The entanglement concentration, C_e, separates the semi-dilute unentangled and the semi-dilute entangled regimes. Above C_e, a steep increase in the zero shear viscosity is observed due to extensive chain entanglements. A rough estimate of C^* and C_e is given by [7-9]

$$C^* \approx \frac{1}{[\eta]} \qquad (1)$$

$$C_e \approx \frac{\rho M_e^{\,0}}{M} \qquad (2)$$

where $[\eta]$ is the intrinsic viscosity, M the molecular mass, ρ the polymer density, and M_e^0 the average molecular mass between entanglements in the undiluted polymer. For the Polystyrene-THF system, it has been shown that chain entanglements become significant when the product of $MC_e \sim 3 \times 10^4$ [10]. The concentrations at which fibers begin to

appear along with beads are shown in Table 1. These values are generally close to the entanglement concentration, C_e. Hence, during electrospinning, stable fibrous structures may typically be observed at $C > C_e$. When $C^* < C < C_e$, a bead dominant morphology may be obtained. As can be expected from eqns. (1) and (2), the transition from bead to fiber occurs at higher concentrations as the molecular weight is decreased. Typically, the transition from bead to bead-free fibers occurs gradually over a range of concentrations [11]. Megelski et al. [2] observed the morphological changes during electrospinning of polystyrene with THF as the solvent. Their results indicate that a bead dominant morphology (with a small fraction of emerging fibers) can be obtained at a concentration of 18 wt%. This concentration corresponds to $\frac{C}{C_e} \sim 2$, where C_e is calculated to be on the order of 10 wt% (based on eqn (2), with ρ = 1.05 g/cm^3 and M_e^0 = 18,100 g/mol [8]). Similar results were obtained in the present investigation, where a bead dominant structure (with emerging fibers) was obtained for $C \sim C_e$. In this case, the beads were highly wrinkled for all molecular weights. Typical examples of wrinkled beads are shown in Fig. 1. The average size of the wrinkled beads increased with molecular weight and concentration and ranged from about 10 to 50 μm. Large wrinkled beads with smooth surface and almost spherical shapes (Fig. 1(a)) were generally obtained at low molecular weight ($M_w \leq$ 44,100 g/mol) solutions at relatively high concentrations (20 ~ 30 wt%). The overall shape and the nature of wrinkles within the beads suggest that a polymer skin may have formed in the early stage of jet disintegration. Localized collapse of this skin may lead to the wrinkled surface shown in Figs. 1(a) and (b). If the skin that forms on the surface develops sufficient strength, it may resist collapse and a hollow bead may be obtained upon solvent evaporation as shown in Fig. 1(c). The

wrinkled beads may also contain numerous surface pores (Fig. 1(b)). The average pore size was on the order of 200 nm, similar to the data of Casper et al. [3] and Megelski et al. [2]. Casper et al. [3] have indicated that pore formation during electrospinning is quite complex and may entail a sequence of events involving phase separation. Further, humidity may play a vital role in pore formation and M_w and polydispersity of the polymer may control the resulting pore diameters.

As the concentration is lowered below C_e, a change in bead morphology may be observed depending on M_w. The wrinkled beads may change to dimpled beads and eventually to cups as the concentration is lowered for M_w = 111,400 and 393,400 g/mol. Figs. 2(a) and (b) show such a transition from dimpled beads to cups observed as the concentration is changed from 16.8 to 11.8 wt%. The shape of the cups was not uniform and shallow cups and dimpled beads were observed in the same sample. Similar results have been reported by Lee et al. [12], who produced cups with polystyrene at M_w = 140,000 g/mol using THF and a concentration of 13 wt%. These results suggest that there may be a range of molecular weights and concentrations in which cups can be produced. Large cups with a porous surface were also observed (Fig. 2(c)). The size of the pores was larger on the inner side of the cup, suggesting that the pore size may depend on the stresses that are caused during the collapse of the bead.

The depth of the cup decreased gradually as the concentration was lowered further, resulting in flat dish-shaped beads (Fig. 3). The decrease in the cup depth upon dilution is consistent with the results reported by Liu et al. [4] Polystyrene dishes were

observed at concentrations ranging from 1 to 8 wt% and M_w between 19,300 and 393,400 g/mol. Higher concentration and molecular weight typically resulted in thicker and larger dishes (Fig. 3). In this concentration regime, toroidal beads were also observed as shown in Fig. 4. The toroidal beads were typically observed with low to moderate molecular weight solutions (19,300, 44,100, and 111,400 g/mol) and were obtained together with dish-shaped beads. Polystyrene dishes typically had rims suggesting that upon collapsing of the drop, the solutions were pushed away to the edge of the beads. As can be seen from Fig. 4(b), it is likely that the holes in the toroids were formed by the radial stress caused by the solvent evaporation from the rim.

Various morphologies such as micro-porous beads, shells, dishes and hollow porous beads can be obtained depending on M_w, as the solution concentration is adjusted to be near C^* (Fig. 5). At low molecular weight (M_w = 19,300 g/mol), the structure consisted predominantly of dishes as shown in Fig. 3(a). In this case, the concentration (1.1 wt%) was slightly below C^*. As M_w is increased to 44,100 g/mol, hollow shells with a smooth surface were obtained at C = 2.6 wt%, just below C^* (Fig. 5(a)). Some beads may collapse to dishes, but many retained nearly spherical shapes. It is likely that after the formation of a thin layer of skin, the atmospheric pressure caused the tears and the holes on the surface thereby creating channels through which the rest of the solvent escaped. Micro-porous beads were produced for M_w = 393,400 g/mol as shown in Fig. 5(b) for C = 2.6 wt% (slightly greater than C^*). The extent of porosity in the micro-porous beads increased as the concentration in this regime was lowered. An extreme

example of the structure at low concentration is shown in Fig. 5(c). In this case, hollow porous beads were produced for C = 0.11 wt% (M_w = 1,877,000 g/mol).

The cumulative effects of molecular weight and concentration on the bead structure are summarized in Fig. 6. Various regions corresponding to different bead morphologies are highlighted. Related works by Megelski et al. [2] and Lee et al. [12] are also indicated. In addition, the dilute solution limit, C^* (calculated from eqn (1) [13]), and the entanglement concentration, C_e (based on the results of Jamieson and Telford [10]), are also shown. In most cases, the transition from one type of bead to the next was gradual and neighboring structures were also observed in the same sample. A general trend in all molecular weight solutions was that upon dilution from a concentration near C_e to below C^*, the morphology of the wrinkles changed into the various structures introduced in this paper. Further investigation is critical in highlighting the mechanism of formation of these beads.

Conclusions

Various bead morphologies including wrinkled beads, cups, dishes, toroids and hollow beads can be produced by controlling the molecular weight and concentration. The surface of the beads can also contain pores on the order of 200 nm. Typically, these bead structures can be obtained from dilute and semi-dilute solutions. Wrinkled beads were obtained from semi-dilute solutions close to the entanglement concentration, C_e, for all

molecular weights. As the concentration was lowered below C_e, other bead morphologies described above were obtained. Micro-porous beads and hollow skeletons were obtained for molecular weights greater than 111,400 g/mol when the concentration was near C^*, the dilute solution limit.

References

[1] S. Koombhongse, W. Liu, D.H. Reneker, J Polym Sci Part B 39 (2001) 2598.
[2] S. Megelski, J. S. Stephens, J.F. Rabolt, D. Bruce Chase, Macromolecules 35 (2002) 8456.
[3] C. L. Casper, J. S. Stephens, N. G. Tassi, D. B. Chase, J. F. Rabolt, Macromolecules 37 (2004) 573.
[4] J. Liu, S. Kumar, Polymer 46 (2005) 3211.
[5] S.L. Shenoy, W.D. Bates, H.L. Frisch, G.E. Wnek, Polymer 46 (2005) 3372.
[6] P. Gupta, C. Elkins, T.E. Long, G.L. Wilkes, Polymer 46 (2005) 4799.
[7] W.W. Graessley, Polymeric liquids and networks: structure and properties, Garland Science, New York, 2004.
[8] J.D. Ferry, Viscoelastic properties of polymers, 3d ed., Wiley, New York, 1980.
[9] E.D.V. Meerwall, E.J. Amis, J.D. Ferry, Macromolecules 18 (1985) 260.
[10] A.M. Jamieson, D. Telford, Macromolecules 15 (1982) 1329.
[11] X. Zong, K. Kim, D. Fang, S. Ran, B.S. Hsiao, B. Chu, Polymer 43 (2002) 4403.
[12] K.H. Lee, H.Y. Kim, H.J. Bang, Y.H. Jung, S.G. Lee, Polymer 44 (2003) 4029.
[13] J. Brandrup, E.H. Immergut, E.A. Grulke, Polymer handbook, 4th ed., Wiley, New York, 1999.

Table I *Experimental conditions used in this study. The weight average molecular weights (M_w) and the corresponding concentration (C) ranges at which experiments were conducted are also shown. The upper limit in concentration at each molecular weight generally corresponds to the onset of fiber formation.*

M_w (g/mol)	C (wt%)
19,300	1.1 ~ 41.8
44,100	1.1 ~ 34.5
111,400	2.6 ~ 21.2
393,400	2.6 ~ 7.5
1,045,000	0.67 ~ 1.3
1,877,000	0.11 ~ 1.0

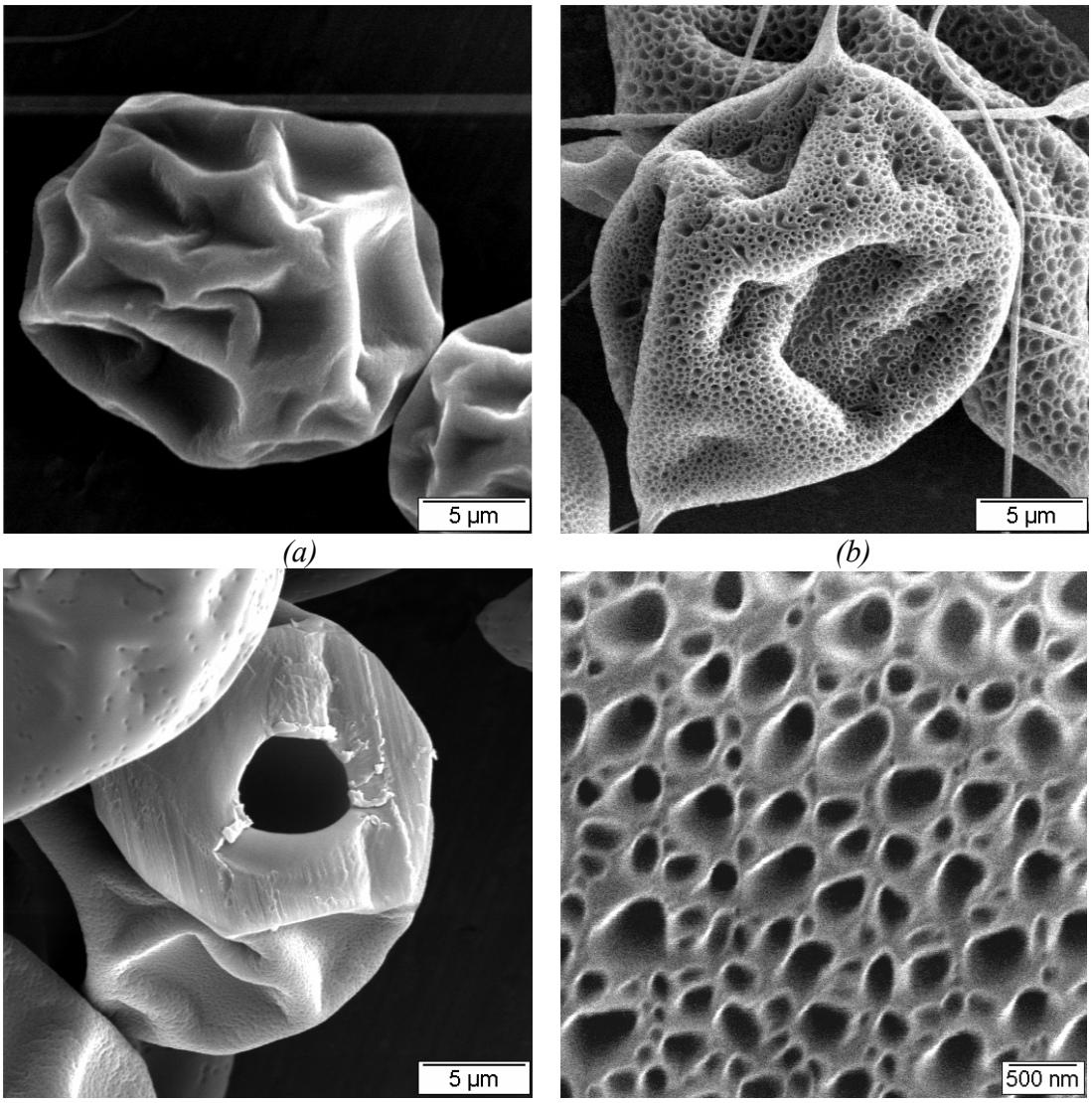

(a) *(b)*

(c) *(d)*

Fig. 1 *Photographs showing solid (a) and porous (b) wrinkled beads. The solid beads have been sliced to reveal a hollow structure inside (c). A high magnification photograph of the surface pore structure in porous beads (b) is shown in (d). ((a) and (c): M_w = 19,300 g/mol, C = 32.4 wt% (b) and (d): M_w = 393,400 g/mol, C = 13.9 wt%.)*

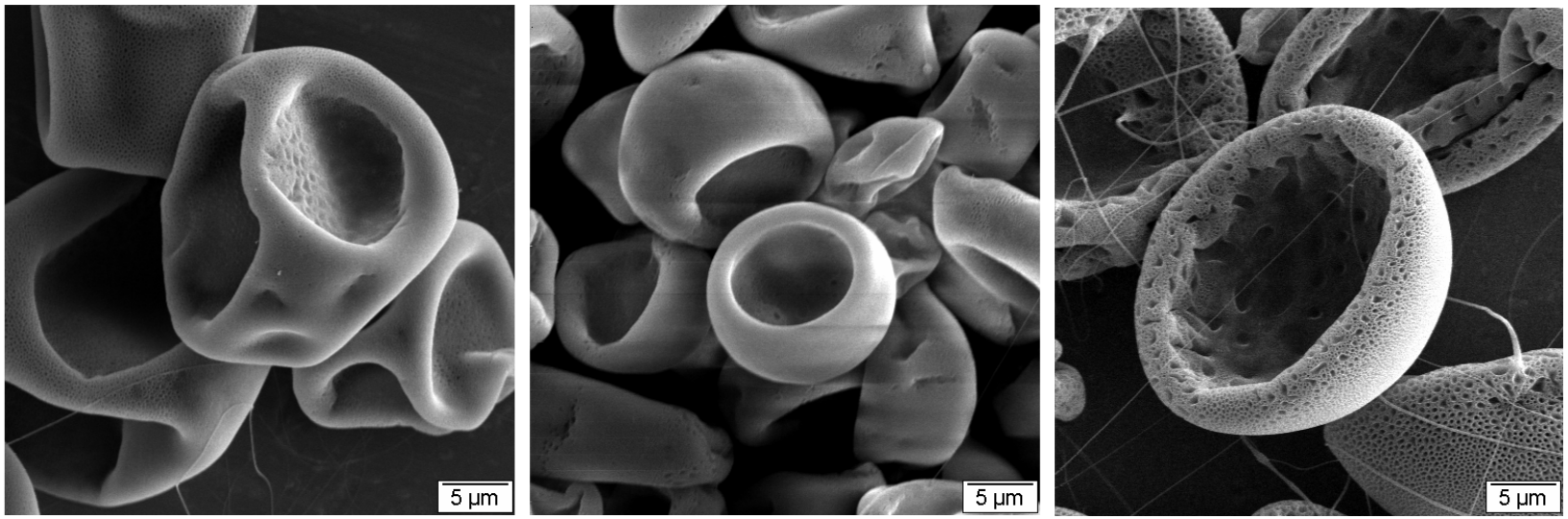

(a) *(b)* *(c)*

Fig. 2. *Photographs showing (a) dimpled beads, (b) non-porous cups and (c) porous cups. (a) M_w = 111,400 g/mol and C= 13.9 wt%, (b) M_w = 111,400 g/mol, C = 11.8 wt%, and (c) M_w = 393,400 g/mol, C = 11.9 wt%.*

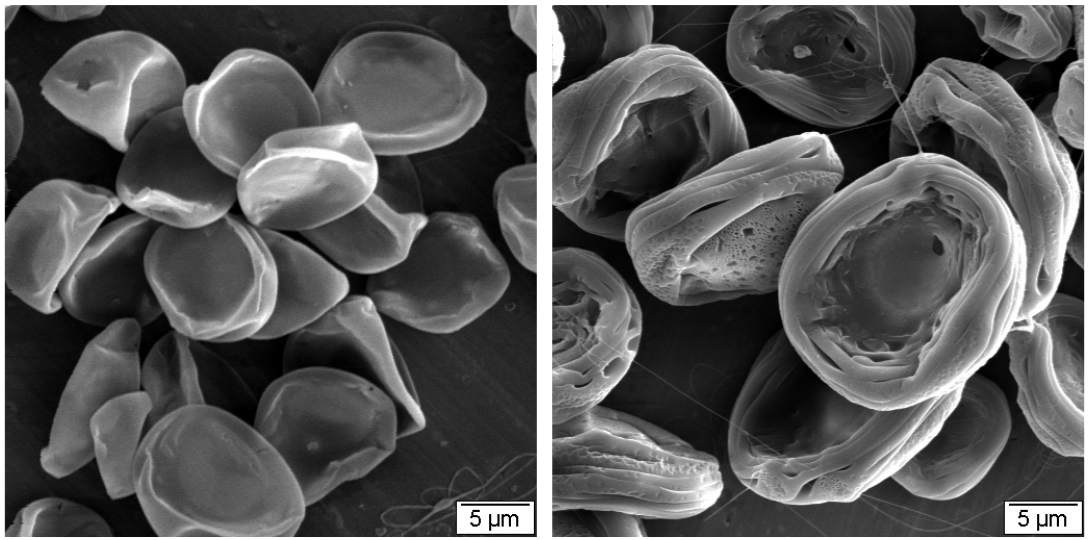

(a) (b)

Fig. 3. Photographs showing dish-shaped beads obtained with a) M_w = 19,300 g/mol, C = 1.1 wt% and b) M_w = 393,400 C = 3.3 wt%. It can be noted that the dish-shaped beads in (b) have a greater wall thickness than in (a).

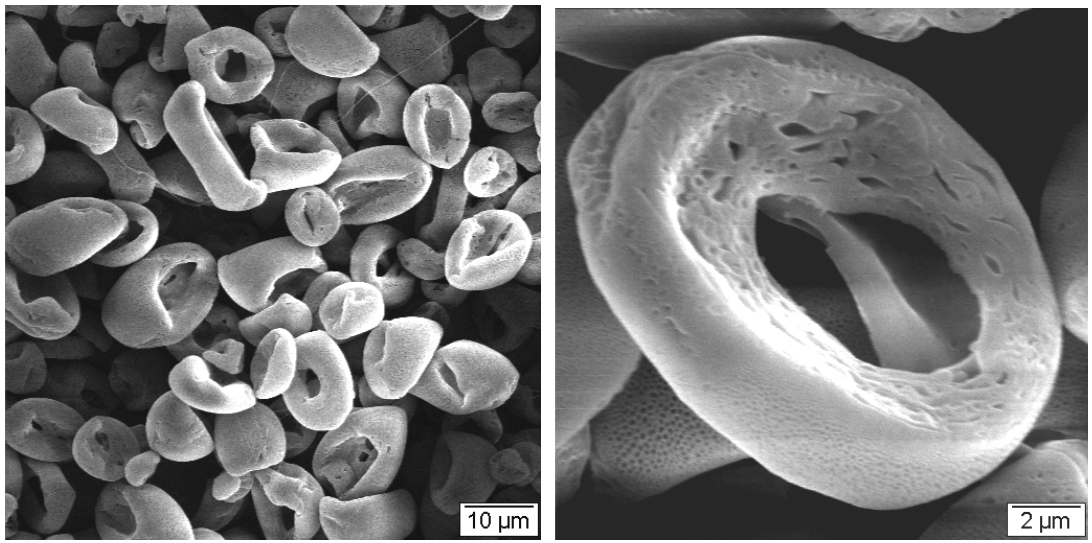

(a) *(b)*

Fig. 4. *Photographs (a) showing the toroidal beads observed at M_w = 111,400 g/mol and C = 6.3 wt%. A high magnification photograph of a single toroidal bead is shown in (b).*

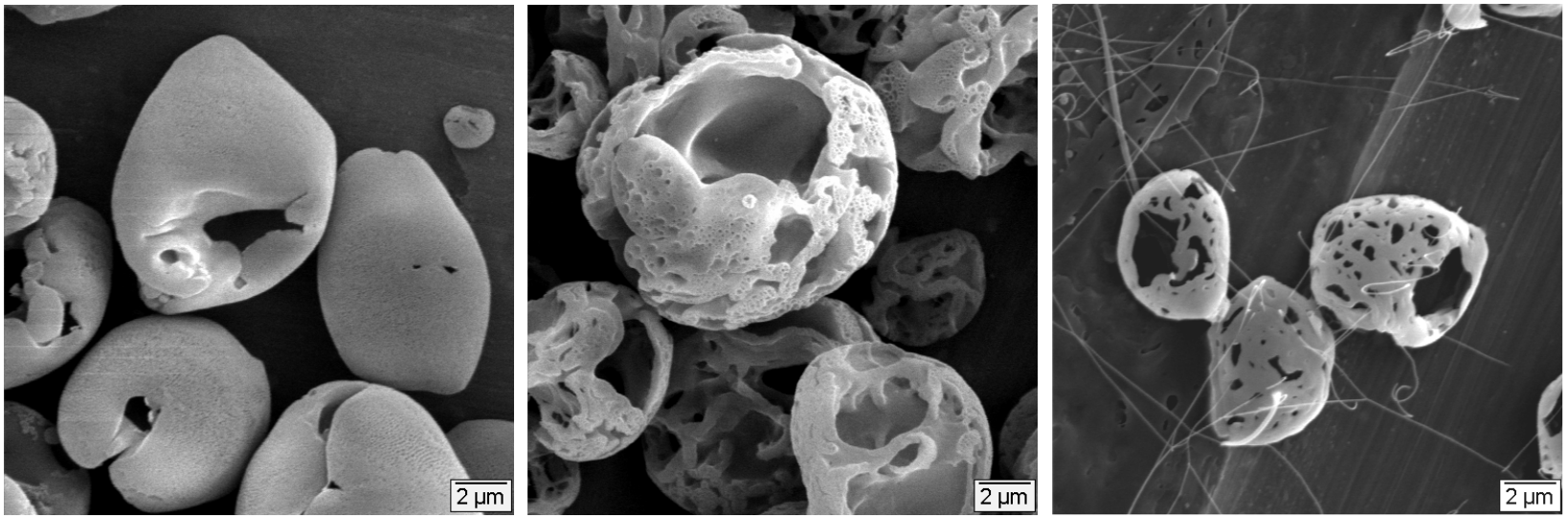

(a) *(b)* *(c)*

Fig. 5. *Photographs showing (a) hollow shells (M_w = 44,100 g/mol, C = 2.6 wt%), (b) micro-porous beads (M_w = 393,400 g/mol, C = 2.6 wt%) and (c) hollow porous beads (M_w = 1,877,000 g/mol, C = 0.11 wt%).*

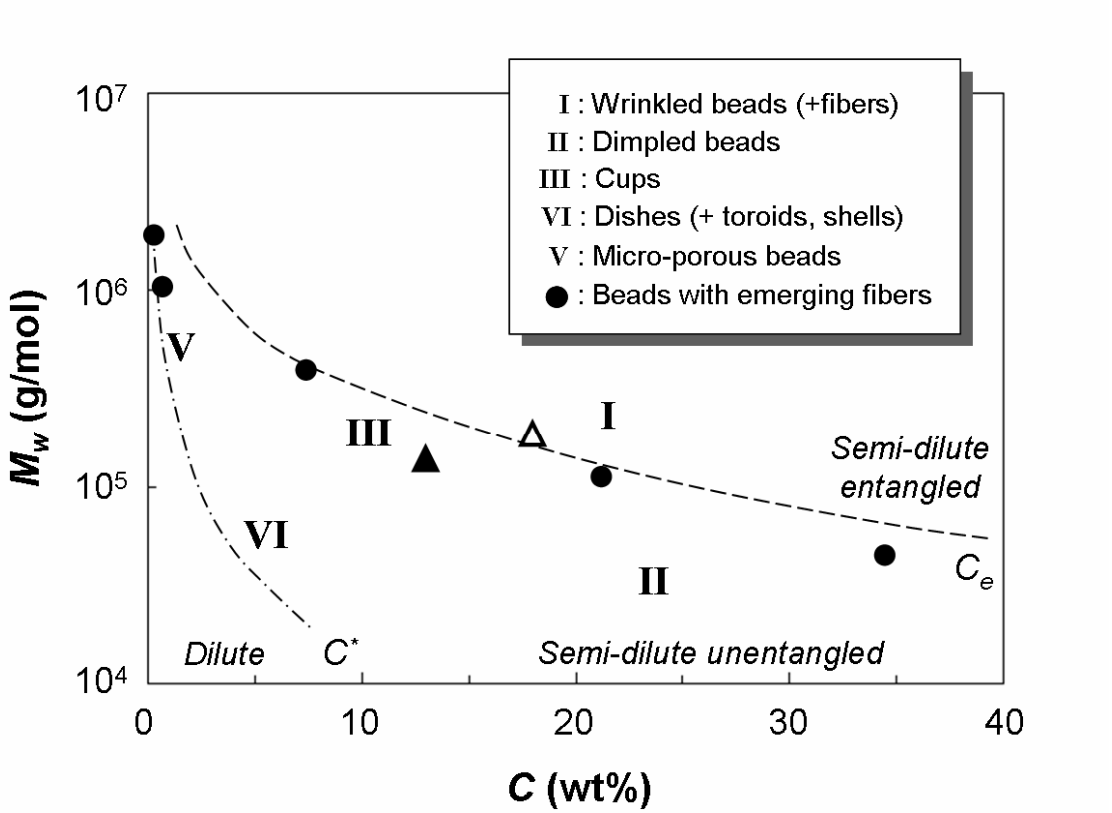

Fig. 6. *Morphological variations in the bead structure as a function M_w and C showing various regimes. The structures shown in parentheses can coexist with the dominant morphology indicated. The limiting concentration at which fibers begin to appear along with beads are also shown for different molecular weights used in this study. The values for the dilute solution limit (C^*) calculated from eqn (1) [13] and the entanglement concentration (C_e) obtained from the data of Jamieson and Telford [10] are plotted. The data of Lee et al. [12] who obtained cups (▲) and Megelski et al. [2] who obtained beads with emerging fibers (Δ) are shown.*

Chapter 2

Bead-to-Fiber Transition in Electrospun Polystyrene

Paper submitted for publication in *Polymer*, 2006

Paper submitted for publication in *Polymer*, 2006

Bead-to-Fiber Transition in Electrospun Polystyrene

Goki Eda and Satya Shivkumar*

Materials Science and Engineering Program,
Department of Mechanical Engineering,
Worcester Polytechnic Institute,
100 Institute Road,
Worcester, MA 01609

Abstract

The morphological transition, namely bead-to-fiber transition, of electrospun polymer was examined for polystyrene with molecular weight ranging from 19,300 to 1,877,000 g/mol. Tetrahydrofuran (THF) and N,N-dimethylformamide (DMF) were used as the solvents to examine the effects of solvent properties on the morphological variations. Polymer molecular weight and solvent properties had a significant effect on the morphology of beads as well as fibers. Observation of fiber diameter and its distribution suggested that the effect of molecular weight and solvent may be independent. The critical concentrations at which incipient and complete fibers were observed were found to decrease significantly with molecular weight, as can been expected. The effect of solvents on these critical concentrations was minimal for moderate to high molecular weight (>100,000 g/mol). For low molecular weight solutions, the transition occurred at concentrations much lower than those predicted by a model based exclusively on chain entanglements. Rapid solidification of jet which is expected to occur with concentrated solutions may play a vital role in establishing stable fibers during electrospinning.

Keywords: Electrospinning; Polystyrene; Molecular Weight; Solvent

**Tel.:* +1 508 831 5048; *fax:* +1 508 831 5178
E-mail address: shivkuma@wpi.edu

Introduction

Despite the large number of articles published over the past decade, the field of electrospinning has not yet reached a stage as a commercially viable option for large scale manufacture of non-woven fibrous structures. The reason traces back to a lack of fundamental understanding of the complex process mechanisms. Often described as an electrohydrodynamics problem [1-4], the study of electrospinning requires an understanding of flow behavior of a viscoelastic polymer solution under an applied electric potential. During the process, a jet of solution ejected from the well-known Taylor cone [5] is subjected to electrical, surface tension, and viscoelastic forces. A dramatic thinning of the jet is achieved through bending, whipping, splitting, and splaying, which are consequences of electrically induced jet instabilities. Concurrent solidification of the jet alters its mechanical properties during the transit of the solution jet from the Taylor cone to the collector. The physical phenomena associated with solvent evaporation, therefore, add to the complexity in modeling efforts [3]. Difficulty in modeling the flow of polymer solution also arises from a lack of available data related to solution rheology. The complexity of the process is reflected in a number of process parameters that affect the morphology of the final product. A large body of research has identified process parameters that have a significant influence on the morphology of electrospun polymers. However, precise tailoring of the electrospun structure for a specific application requires an understanding of not only the influence of each process parameter but also their cumulative effects.

The structure of electrospun polymer ranges from particulate (in which case the process may also be referred to as "electrospraying") to fibers depending on various conditions [6]. In between these extremes, a combination of these morphologies may result in beaded fibers [7,8], which are often considered as structural defects. As attractive features of electrospinning, these structures may also exhibit wide variations in their shapes and surface morphologies [9-12]. Some of the recent studies have focused on the transition of these structures, namely the bead-to-fiber transition, with respect to the rheological properties of polymer solutions. McKee et al. [13] and Gupta et al. [14] investigated morphological transitions based on critical hydrodynamic concentrations, *i.e.* the entanglement concentration (C_e) and the chain overlap concentration (C^*), respectively. Their results indicate that stable fibers start to form for solutions in the semi-dilute-entangled regime. Shenoy et al. [15] employed a semi-empirical approach in establishing a model for bead-to-fiber transition based on chain entanglement analysis. According to their model, the minimum requirement for the formation of some fibers is one entanglement per polymer chain, whereas, more than 2.5 entanglements per chain may be required to form bead-free fibers. The relative comprehensiveness of this model has been indicated by examining the applicability to several polymer-solvent systems.

While the importance of chain entanglements has been recognized, other solution properties are also known to play an important role in determining the morphology of electrospun polymers [7,16,17]. For instance, it is well known that a solution with a high charge density results in a fine fiber structure due to the large extensional force in a jet of solution [18]. Since the solvent used determines solution properties to a large extent,

several investigators have explored the change in morphology of polymers electrospun from various solvents [16-23]. Many reports have shown that the use of solvents with a large dielectric constant and electrical conductivity typically results in increased uniformity and reduced number of beads in the electrospun fibers [19,20,23]. The addition of salts [6,7] and surfactants [24] is also known to demonstrate a similar effect. However, a quantitative study of these parameters remains difficult as the effect of solvent properties cannot be isolated. Recently, Larsen et al. [25] were successful in isolating the effect of evaporation rate by the use of a coaxial gas jacket. Their results show that by controlling the evaporation of volatile solvents, bead-to-fiber transitions can be induced. It is implied that the formation of stabilizing junctions within the jet of solution by solvent evaporation plays a vital role in determining the resulting polymer structure. In this case, bead-to-fiber transition is not solely dependent on the entanglement number.

The morphology of electrospun polymer, therefore, may be controlled by various parameters. In order to predict the resulting structure for a given condition, the contribution of rheological and other effects must be considered. In this study, the cumulative effects of fundamental solution parameters such as polymer molecular weight, concentration, and solvent properties on the morphological variations within the electrospun polymer were investigated. A wide range of polymer molecular weights was examined to investigate the applicability of a previously proposed model based on chain entanglement in extreme conditions [15]. Solvents with contrasting properties were used to explore non-rheological effects on morphological transitions.

Experimental procedure

Linear atactic polystyrene (PS) with six different weight average molecular weights (M_w) ranging from 19,300 to 1,877,000 g/mol and polydispersity index of about 1 was obtained from Scientific Polymer Products (Ontario, NY) and used without further purification. Solutions were prepared by dissolving the polymer in tetrahydrofuran (THF) (Sigma-Aldrich) and N,N-dimethylformamide (DMF) (Sigma). Both solvents were reagent grade.

In order to determine the transition concentration (*i.e.* bead-to-fiber) for each molecular weight, electrospinning was conducted for several solution concentrations varying in steps of ~1 to 4 times the dilute solution limit for PS in THF (C^*_{THF}), which was calculated according to [26]:

$$C^*_{THF} = \frac{1}{[\eta]_{THF}} = \frac{1}{0.011 M_w^{0.725}} \qquad (1)$$

where $[\eta]_{\mathrm{THF}}$ is the intrinsic viscosity of PS in THF in mL/g, with 0.011 and 0.725 being the corresponding Mark-Houwink constants [27]. The same concentrations were used for the two systems in order to highlight the effects of the solvent. About 0.5 mL of solution with the desired concentration was prepared and drawn into a 1 mL syringe equipped with an 18 gauge needle (inner diameter = 0.84 mm, 51 mm long). The syringe was placed horizontally on a syringe pump (EW-74900-00, Cole-Parmer), which was calibrated to deliver the solution to the needle tip at a rate of 3 and 1 mL/hr for PS-THF and PS-DMF systems respectively. A grounded aluminum foil collector (10 cm × 10 cm)

was positioned 10 cm from the tip of the needle. In most experiments, a potential of 10 kV was applied to the needle during electrospinning. A limited number of experiments were also conducted at a voltage of 30 kV to highlight the effects of the applied potential on the electrospun morphology. The whole apparatus was enclosed in a Plexiglas box, which was constantly evacuated during the process to control solvent evaporation. The electrospun polymer was dried for at least a day and sputter-coated for scanning electron microscope (JSM-840) examination. Fiber diameter distribution was obtained using a commercial software package, AnalySIS® (Soft Imaging System, CO).

Results and Discussion

The extent of chain entanglements in the solution can be characterized by various parameters. The critical concentrations such as C^* and C_e are often employed to describe the degree of overlap of hydrodynamic volumes in which polymer molecules are confined. The limiting concentration for dilute solution, C^*, is determined to some extent by the solvent quality as the approximate value of C^* can be expressed as the inverse of intrinsic viscosity [26]. Therefore, the value of C^* may be smaller for a good solvent than for a poor solvent. The expression for the entanglement concentration, C_e, for a good solvent is [28]:

$$C_e \approx \frac{\rho M_e}{M_w} \qquad (2)$$

where ρ the polymer density and M_e is the entanglement molecular weight of the undiluted polymer. Above C_e, a sharp increase in zero shear viscosity is observed due to extensive chain entanglements. For the PS-THF system, Jamieson and Telford [29] observed this upturn in viscosity to occur for $M_w C_e \sim 3 \times 10^4$. This criteria yields a value of C_e larger than that obtained from eqn (2) by a factor of about two using ρ = 1.05 g/cm^3 and M_e = 16,600 g/mol [15]. McKee et al. [13] showed that during electrospinning, C_e is the minimum concentration required for the formation of beaded fibers, whereas 2~2.5 times C_e may be required for the formation of bead-free fibers. In a similar manner, Shenoy et al. [15] evaluated the bead-to-fiber transition in terms of the solution entanglement number, $(n_e)_{soln}$, which is a ratio of the polymer molecular weight to its solution entanglement molecular weight, $(M_e)_{soln}$. Using the relationship, $(M_w)_{soln} = M_e/\phi_p$ [28], where ϕ_p is the polymer volume fraction, the solution entanglement number is

$$(n_e)_{soln} = \frac{\phi_p M_w}{M_e}. \qquad (3)$$

It can be noticed that eqns (2) and (3) are essentially equivalent for $(n_e)_{soln}$ = 1. According to the analysis of Shenoy et al. [15], the transition in the morphology of electrospun polymer can be predicted by this parameter. The onset of fiber formation, for instance, can be estimated to occur for conditions corresponding to $(n_e)_{soln}$ = 2. In terms of C_e, the corresponding concentration is $2C_e$ according to eqn (2), or C_e according to $M_w C_e \sim 3 \times 10^4$. Similarly, complete fibers are expected to form when $(n_e)_{soln} \geq 3.5$.

PS-THF system

During electrospinning, the morphological transition from bead-only to bead-free structure takes place gradually over a range of polymer concentrations. Megelski et al. [10] have shown the transition from bead dominant structure to bead-free fibers for PS with M_w = 190,000 g/mol electrospun from THF. In this case, the transition was shown to take place for concentrations between 18 and 35 wt%. As has been discussed by Shenoy et al. [15], these concentrations correspond to $(n_e)_{soln}$ = 2 and 3.5, indicating the onset of initial fiber formation and bead-free fiber formation respectively. Their optical micrographs of the electrospun polymer show that during this transition, the number of beads reduces and the fiber diameter increases with concentration. The general trend of morphological variations observed in the present study was consistent with the results reported to date. SEM photographs of the onset of incipient fiber formation and morphological variation of beads and fibers for M_w = 393,400 g/mol electrospun from THF are shown in Fig. 1. For concentrations well below C_e, which was estimated to be 7.9 wt% (according to $M_w C_e \sim 3 \times 10^4$ [29]), the amount of chain entanglement was negligible and structures consisting only of beads were obtained (Fig. 1(a)). The types of beads shown in Fig. 1 correspond to the range of structures described in our previous work [12], where a transition from micro-porous to dish-shaped beads was documented. When the concentration was increased near C_e, incipient fibers emerging from some beads were observed in small fractions (Fig. 1(b)). Although some isolated beads were observed, the formation of these incipient fibers suggests some degree of chain entanglement in the solution. The solution entanglement number, $(n_e)_{soln}$, calculated for

this condition was 1.5, which is in good agreement with the prediction from Shenoy et al.'s model [15]. The fraction of incipient fibers increased with concentration (Fig. 1(c)). In this regime, the structure of beads varied significantly and the formation of cups with sub-micron pores was observed. Further increase in concentration resulted in a continuous structure in which all beads were connected by fibers (Fig. 1(d)). Above this concentration, the occurrence of beads diminished and their shape became more spindle-like (Figs. 1(d) and (e)) until complete fibers (Fig. 1(f)) were formed. These results are in agreement with the data reported previously [20]. PS fibers electrospun from THF typically had a non-circular cross-section (Fig. 1(f)). The formation of flat fibers was discussed by Koombhongse et al. [9]. It is expected that the high evaporation rate of THF may have contributed to skin formation and collapse of the hollow tube leading to flat fibers. The typical aspect ratio was measured to be 2.4. The ridges and surface undulations observed on some fibers suggest that they may be in the process of splitting [9]. For the PS-THF system, fused structures were typically observed for extremely low concentrations (C < 1 wt%) as well as for relatively high concentrations at which fibers were produced (Fig. 2). The fiber mat shown in Fig. 1(f) also contained some fused fibers at different parts of the sample (Fig. 2 (b)) indicating incomplete evaporation of the solvent as the solution jet reached the collector. This observation suggests that two competing factors may contribute to the complete evaporation of the solvent. As the fraction of solvent in the solution is increased, the time it takes for complete evaporation is extended beyond the "flight time," thereby leaving fused structures. On the other hand, as the fraction of solvent is lowered such that only fibers are formed, the effective surface area available for the solvent to evaporate is reduced (as the surface area of fibers is less

than that of beads) and complete evaporation is inhibited. It can also be noted that the formation of a skin (often observed for high concentration) may retard solvent evaporation as the solvent molecules diffuse much more slowly within the skin. Based on these transitions, it can be concluded that for M_w = 393,400 g/mol, the onset of incipient fiber formation occurs at C = 7.5 wt% and bead-free fibers are stabilized for C = 21.2 wt%. For convenience, these critical concentrations are denoted by C_i and C_f respectively. Hence, C_i corresponds to the onset of fibers from beads and C_f is the lowest concentration at which a completely fibrous structure is stabilized. Since an increase in concentration results in thicker fibers, C_f may be considered as the lowest concentration at which bead-free fibers with the smallest diameter may be obtained. C_i and C_f are functions of M_w, as can be expected. However, it should also be noted that a change in the electric field strength may shift these values. To illustrate this point, a solution with a concentration slightly below C_i and C_f was electrospun at a voltage of 10 and 30 kV (Fig. 3). Comparing Figs. 3(a) and (b) (where the same concentration was used), it is apparent that incipient fiber formation is easier at a higher voltage. The underlying mechanism for this phenomenon is not readily evident, however, the rheological properties of the solution may have been altered by the large change in the electric field as previous studies have shown [30-32]. An example of bead elimination from beaded fibers when the voltage is increased is shown in Figs. 3 (c) and (d). The absence of beads in Fig. 3(d) may be a result of the increased extensional force in the jet induced by increased electric field. Although a large potential may decrease the critical concentrations, too high an electric field is typically not preferred due to defect formation and loss of morphological

uniformity [10]. Further examination of the variation of C_i and C_f were conducted at a fixed applied voltage (10 kV).

The reduction in polymer molecular weight significantly increased the concentrations at which morphological transitions took place. For M_w = 19,300 g/mol, a bead-only structure was obtained for concentrations as high as 32.4 wt%, suggesting the lack of chain entanglement in the solution (Fig. 4(a)). Nevertheless, continuous structures began to form upon increasing the concentration (Fig. 4(b)). For conditions corresponding to the bead-free fiber formation regime, the calculated $(n_e)_{soln}$ was less than 1 for low molecular weight solutions (19,300, 44,100 g/mol). Although the applicability of Shenoy et al.'s [15] model at these high concentrations may be questioned, the formation of complete fibers with M_w = 19,300 g/mol, which is just above the entanglement molecular weight of 16,600 g/mol [15], was unexpected. The formation of fibers for low molecular weight solutions may be attributed to the rapid solidification of the jet. For concentrated solutions (C > 30 wt%), evaporation of a small amount of solvent may lead to immediate skin formation. It may be speculated that the solution jet ejected from the Taylor cone undergoes solidification before Rayleigh instability can take effect. In fact, when concentrations higher than 30 wt% were used, the solution solidified immediately after emerging from the capillary and often terminated the electrospinning process in a few seconds. In the beaded-fiber regime, the amount of incipient fibers increased with molecular weight suggesting enhanced contribution of chain entanglements (Fig. 4(b), (e) and (h)). However, the fact that complete fibers are

observed for $(n_e)_{soln}$ of 1.7 rather than the predicted value (≥ 3.5) for M_w = 111,400 g/mol suggests that solvent evaporation may have played a dominant role in jet stabilization.

A bead-to-fiber transition was observed at lower concentrations as the molecular weight is increased. For M_w > 1,000,000 g/mol, a bead-to-fiber transition was observed at C < 12 wt%. Further, when M_w > 1,000,000 g/mol, the bead-only regime was not observed even for the lowest concentration used in this study (0.01 wt%). Some incipient fibers were present even for $C < C^*$ as shown in Fig. 5 indicating the presence of chain entanglements in the solution. It is possible that high molecular weight polymers were not completely dissolved in the solvent and domains of entangled molecules that remain in the solution may facilitate fiber formation. The variation of bead morphology was similar to the behavior observed with other molecular weights. At concentrations just above C^*, the beads typically had dish-shapes as shown in Fig. 5 (b). A slight increase in concentration resulted in cup-shaped beads with a smooth surface (Fig. 6(a) and (d)). At higher concentrations, spindle-shaped, wrinkled beads were observed (Fig. 6(b) and (e)). This transition suggests the formation of a thick and stiff skin at the bead surface induced at high concentrations. The bead-free fibers, obtained with high molecular weight polymer, were also flat with an average aspect ratio of about 2.8, which did not vary significantly with molecular weight.

The variation of fiber diameter is generally consistent with previous reports *i.e.* the fiber diameter increases with C or M_w, when the other parameter is held constant. In this study, the fiber diameter distribution at C_f for different molecular weights was

examined (Fig. 7). Note that the fiber distribution shown in Fig. 7 corresponds to the lowest concentration at which a bead-free fibrous structure was observed. The average fiber diameter significantly decreased with increasing molecular weight at these concentrations. Further, the distribution shifts towards smaller diameters. This result may be explained by the large difference in the values of $[\eta]$, which is analogous to the size of the hydrodynamic volume. A polymer with large $[\eta]$ defines a large hydrodynamic sphere with extensive coiling. Entanglements are readily formed at a low concentration and extensional deformation is likely to occur by uncoiling of the chains. The amount of polymer required to stabilize a unit length of fiber may thus be minimal. As a result, if the polymer concentration is optimized, the fiber diameter may be smaller for high molecular weight polymers. The multimodal fiber distribution reported previously by many investigators [33,34] was also observed in this study.

PS-DMF system

DMF is a moderately good solvent for PS with Mark-Houwink constants $K = 31.8$ mL/g and $a = 0.603$ [27]. The use of DMF in electrospinning has been reported by many investigators [16-21]. DMF is a polyelectrolytic solvent with relatively high dielectric constant (36.4) compared to that of THF (7.6). The primary effect of using DMF instead of other electrically "poor" solvents is the reduction in fiber diameter due to increased elongational force within the solution jet. Lee et al. [20] observed the reduction of beads at a condition in the beaded fiber regime when DMF was used in place of THF during

electrospinning of polystyrene. One of the principal observations from this study which showed a reduction in fiber diameter and bead formation with a change in solvent from THF to DMF was in general agreement with several previous reports [19-21]. The bead-to-fiber transition for M_w = 393,400 g/mol is shown in Fig. 8. At C = 2.5 wt%, the electrospun structure consisted of beads only (Fig. 8(a)). The beads obtained at this condition formed a rough surface that was unlike any of those observed with the PS-THF system. This type of surface was typically observed for solutions with low concentrations (< 5 wt%). Upon increasing the concentration, an incipient fiber regime was observed (Fig. 8(b)). Compared to the data for the PS-THF system, the fraction of incipient fibers is high at this stage. A further increase in concentration resulted in the formation of beaded and bead-free fibers (Figs. 8(c) and (d)). The critical concentrations, C_i and C_f, for M_w = 393,400 g/mol in PS-DMF system were determined to be 4.8 and 20.2 wt% respectively. In comparison with the data for THF as the solvent, C_i and C_f, are very similar. Considering the fact that DMF is not as good a solvent for PS as THF, it may be assumed that the difference in solvent quality exhibited between THF and DMF may not have a significant effect on the morphological transitions for this molecular weight. The fact that the values of C_f obtained from two systems were similar was also unexpected as DMF is known to reduce the fraction of beads [20] as mentioned earlier. In fact, in most cases, the number and the size of beads on the fibers were reduced. However, complete removal of beads from the fibers required concentrations comparable to C_f in the PS-THF system.

The variations in bead and fiber morphology were limited when DMF was used as the solvent (Fig. 9) unlike the case with the PS-THF system. Typically, the beads obtained with DMF for $C < C_i$ were nearly spherical and formed a smooth surface unlike the wrinkles observed with THF. This may be the result of the low evaporation rate of DMF. THF having lower boiling point and heat of vaporization compared to DMF is expected to evaporate at a much slower rate. Immediate evaporation of the solvent may induce skin formation and collapse, which results in the shape variation of beads and fibers. Despite the large difference in evaporation rate between the two solvents, fused structures (indicative of incomplete solvent evaporation), that were often observed with the PS-THF system, were rarely observed in the PS-DMF system. This result may be attributed to the fine structures obtained with DMF as the solvent. By comparing Figs. 4 and 9, for example, it can be noticed that beads and fibers obtained with DMF as the solvent are almost an order of magnitude smaller than those produced with THF. Therefore, the total area from which the solvent can evaporate should be an order of magnitude larger.

The increase in C_i and C_f with decreasing molecular weight was similar to that of the PS-THF system, however, the transitions did not occur at the same concentrations. For Mw = 19,300 g/mol, a bead-only structure was observed for concentrations up to 40 wt% (Fig. 9 (a)). It may be recalled that at this concentration, some fibers may start to form for the PS-THF system (Fig. 4 (b)). Beaded fibers for this molecular weight were observed for C = 47.3 wt%, at which concentration bead-free fibers could be seen with THF (Fig. 4(c)). In other words, at this molecular weight and concentration, the use of

DMF promoted the formation of beads rather than suppressing their presence. This behavior may again be attributed to the difference in evaporation between the two solvents. When DMF is used as the solvent, complete solidification takes place after Rayleigh instability develops. In this concentration regime where solidification is rapid, the effect of high charge density in removing beads may be minimal.

High molecular weight solutions (M_w = 1,045,000, 1,877,000 g/mol) resulted in structures containing some fibers for all concentrations examined (Fig. 10). For M_w = 1,045,000 g/mol, the transition from beaded to bead-free fibers occurred at C = 11.2 wt%, which was essentially the same as the value obtained for PS-THF system. For M_w = 1,877,000 g/mol, however, bead-free fibers were obtained for concentration as low as 0.8 wt%, which is significantly lower than values of C_f obtained for other conditions. The normalized critical concentration, $\frac{C_f}{C^*}$, for M_w = 1,877,000 g/mol, is about 1.5, whereas the corresponding value is calculated to be above 12 for all other conditions. The reason for this sudden drop of C_f with respect to molecular weight is not readily evident, however, the large difference in $\frac{C_f}{C^*}$ suggests that the mechanisms involved in yielding bead-free fibers may have been different in this particular case. The fiber diameter distribution of PS-DMF systems at C_f is shown in Fig. 11. At C_f, an increase in molecular weight significantly reduced the fiber diameter and shifted the overall distribution to smaller diameters, similar to the results with the PS-THF system. The use of DMF as the solvent typically resulted in unimodal fiber distribution. This result is

consistent with previous reports on the fiber distribution in other electrospun polymers [19,21].

The variation of C_i and C_f as a function of molecular weight for both solvents is shown in Fig. 12. For high molecular weights where bead-only structure was not observed, the lowest concentration examined in this study was taken as C_i. Relevant data from previous reports [10,20] are also shown for comparison. The predicted transition concentration for PS-THF system based on the solution entanglement number model [15] is indicated. It is apparent that the deviation from the prediction is significant for molecular weights below 100,000 g/mol. As mentioned earlier, for these molecular weights, fiber formation may be facilitated possibly due to the rapid solidification of the jet owing to high polymer concentrations. The difference in the values of C_i and C_f for the two systems is minimal for most cases. At low to moderate values of M_w ($\leq$ 111,400 g/mol), C_i and C_f are slightly larger for the PS-DMF system than for the PS-THF system, suggesting that fiber stabilization may have been impeded by the low evaporation rate of DMF.

Fiber diameter

Extensive theoretical and experimental analysis has shown the fiber diameter to depend on both molecular weight and concentration. It has been shown that fiber diameter may be correlated with critical concentrations, C^* and C_e [13,14]. In this study,

a different approach was taken to evaluate the effect of molecular weight. The variation of fiber diameter as a function of molecular weight for $C = C_f$ is shown in Fig. 13. The fiber distribution is plotted at the minimum concentration at which bead-free fibers were observed. At this condition, the average fiber diameter decreases consistently with molecular weight for both systems. Interestingly, for both systems, the fiber diameter obeys a power law relationship with molecular weight with an exponent of -0.5. This result suggests that the effect of molecular weight may be independent of solvent properties. A similar tendency is observed in the results of Gupta et al. [14] who examined PMMA-DMF system for a range of molecular weight. Relevant results selected from their work are plotted in Fig. 13 for comparison. The data of Megelski et al. [10] (also shown in Fig. 13) diverges slightly from the results obtained in this study, perhaps due to different processing conditions, such as applied electric field and working distance.

Conclusions

The morphology of electrospun polystyrene depends significantly on polymer molecular weight, concentration and solvent. The morphological transitions from bead-dominant structure to bead-free fibers can be characterized by two critical concentrations, C_i and C_f. These values decrease considerably with increasing molecular weight due to the chain entanglement effect. The applied voltage may also influence the transition. The solvent has minimal effect on the critical concentrations for M_w > 100,000 g/mol.

The transition concentrations are generally consistent with the prediction of entanglement model proposed by Shenoy et al. [15] for M_w > 100,000 g/mol. However, for M_w < 100,000 g/mol, fibrous structures may be obtained at concentrations appreciably lower than those predicted by their model. For solutions with high concentration (C > 30 wt%), fibers may be partially stabilized through rapid jet solidification during the initial stages. The use of a volatile solvent may facilitate fiber formation.

The morphology of beads and fibers varies noticeably with the PS-THF system, perhaps owing to the rapid evaporation of the solvent. Fibers electrospun from THF are typically flat and have diameters an order of magnitude larger than those obtained with DMF. The average fiber diameter decreases significantly with molecular weight for conditions corresponding to $C = C_f$, which is the minimum concentration for bead-free fiber formation. At this condition, the average fiber diameter may be considered as the minimum for a given molecular weight and the accompanying process conditions. The average fiber diameter for $C = C_f$ was found to be proportional to $M_w^{-0.5}$ regardless of the solvent.

References

[1] Reneker DH, Yarin AL, Fong H, Koombhongse S. J Appl Phys 2000;87:4531-47.
[2] Hohman MM, Shin M, Rutledge G, Brenner MP. Physics of Fluids 2001;13:2201-20.
[3] Yarin AL, Koombhongse S, Reneker DH. J of Appl Phys 2001;89(5):18-3026.
[4] Feng JJ. J Non-Newtonian Fluid Mech 2003;116(1):55-70.
[5] Taylor GI. Proc Roy Soc Lond A 1969;313:453.
[6] Zong X, Kim K, Fang D, Ran S, Hsiao BS, Chu B. Polymer 2002;43(16):4403-12.

[7] Fong H, Chun I, Reneker DH. Polymer 1999;40(16):4585-92.
[8] Zuo W, Zhu M, Yang W, Yu H, Chen Y, Zhang Y. Polym Eng Sci 2005;45(5):704-9.
[9] Koombhongse S, Liu W, Reneker DH. J Polym Sci Part B: Polym Phys 2001;39(21):2598-06.
[10] Megelski S, Stephens JS, Rabolt JF, Chase DB. Macromolecules 2002;35(22):8456-66.
[11] Liu J and Kumar S. Polymer 2005;46(10):3211-4.
[12] Eda G and Shivkumar S. J Mater Sci 2006; accepted for publication.
[13] McKee MG, Wilkes GL, Colby RH, Long TE. Macromolecules 2004;37:1760-7.
[14] Gupta P, Elkins C, Long TE, Wilkes GL. Polymer 2005;46(13):4799-10.
[15] Shenoy SL, Bates WD, Frisch HL, Wnek GE. Polymer 2005;46(10):3372-84.
[16] Lee KH, Kim HY, Khil MS, Ra YM, Lee DR. Polymer 2003;44(4):1287-94.
[17] Son WK, Youk JH, Lee TS, Park WH. Polymer 2004;45(9):2959-66.
[18] Yang Q, Zhenyu LI, Hong Y, Zhao Y, Qiu S, Wang CE, Wei Y. J Polym Sci Part B: Polym Phys 2004;42(20):3721-6.
[19] Lee KH, Kim HY, La YM, Lee DR, Sung NH. J Polym Sci, Part B: Polym Phys 2002;40(19):2259-68.
[20] Lee KH, Kim HY, Bang HJ, Jung YH, Lee SG. Polymer 2003;44(14):4029-34.
[21] Hsu CM and Shivkumar S. Macromol Mater Eng 2004;289(4):334-40.
[22] Wu X, Wang L, Yu H, Huang Y. J Appl Polym Sci 2005;97(3):1292-7.
[23] Eda G, Liu J, Shivkumar S. Eur Polym J 2006; under review.
[24] Lin T, Wang H, Wang H, Wang X. Nanotechnology 2004;15(9):1375-81.
[25] Larsen G, Spretz R, Velarde-Ortiz R. Adv Mater 2004;16(2):166-9.
[26] Graessley WW. Polymeric liquids and networks : structure and properties. New York: Garland Science; 2004.
[27] Brandrup J, Immergut EH, Grulke EA. Polymer Handbook. 4th Ed. New York: Wiley; 1999.
[28] Ferry JD. Viscoelastic properties of polymers 3rd Ed. New York: Wiley; 1980.
[29] Jamieson AM and Telford D. Macromolecules 1982;15:1329-32.
[30] Price C, Deng N, Lloyd FR, Li H, Booth C. J Chem Soc Faraday Trans 1995;91(9):1357-62.
[31] Wang CH and Huang QR. J Chem Phys 1997;106(7):2819-23.
[32] Sun Z and Wang CH. Macromolecules 1999;32(8):2605-9.
[33] Deitzel JM, Kleinmeyer J, Harris D, Tan NCB. Polymer 2001;42(1):261-72.
[34] Hsu C-M and Shivkumar S. J Mater Sci 2004;39(9):3003-13.

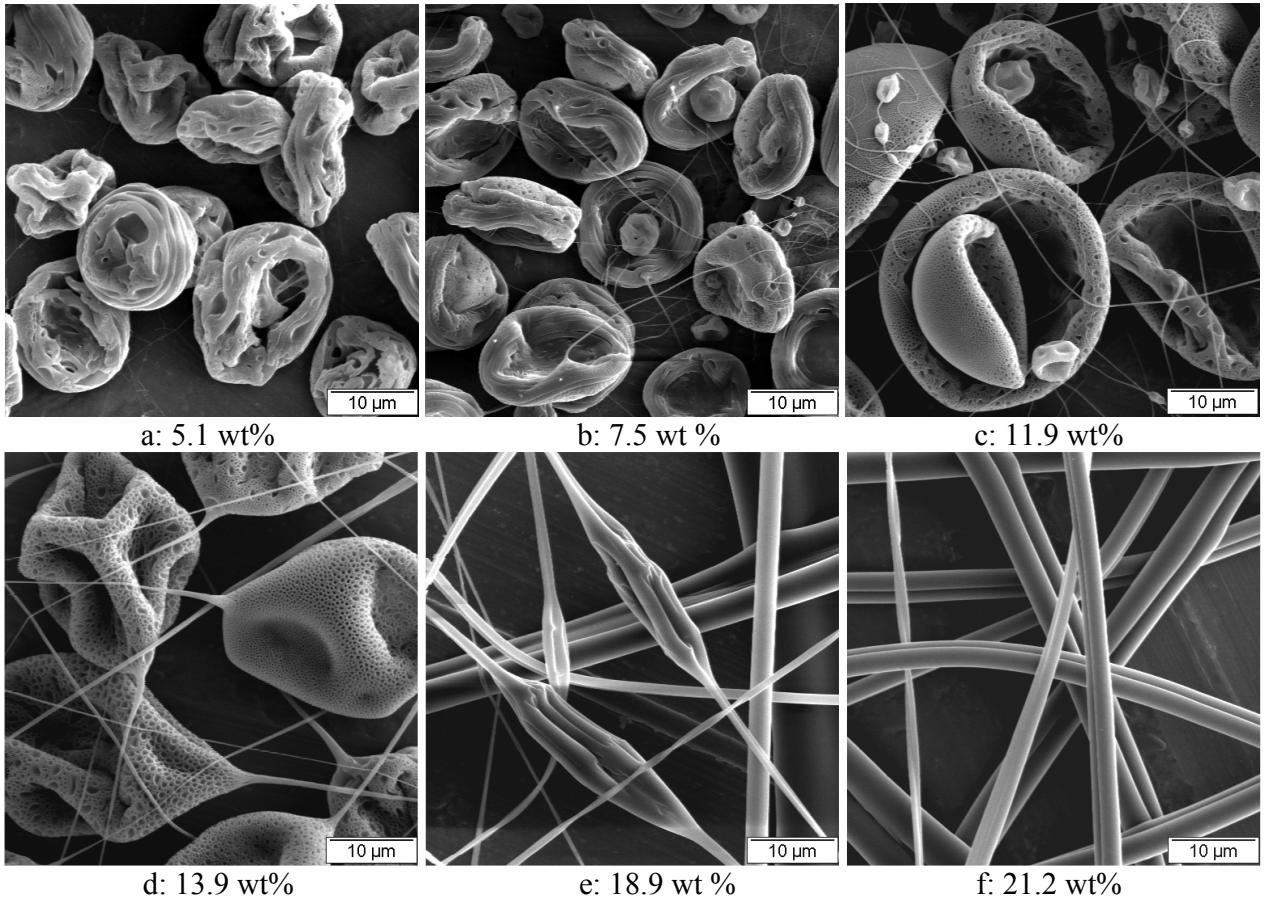

Fig. 1. SEM photographs showing different structural regimes during bead-fiber transition. As the concentration is increased, the morphology consists of (a) beads only, (b,c) beads with incipient fibers, (d,e) bead-on-string, and (f) bead-free fibers (M_w = 393,400 g/mol). The corresponding solution concentrations are indicated.

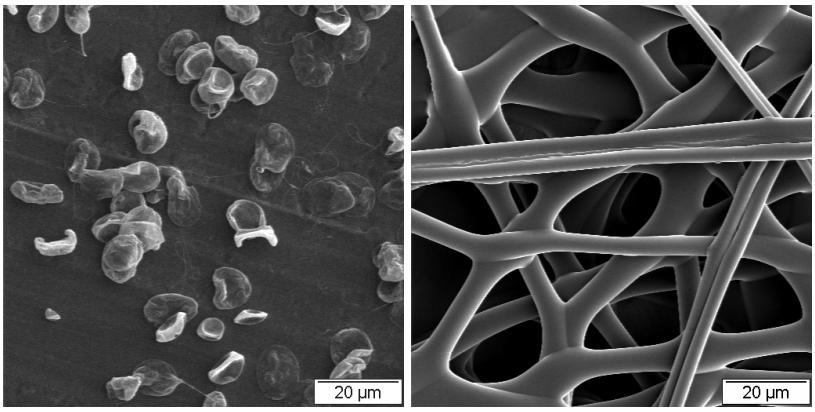

a: 0.1 wt % b: 21.2 wt%

Fig. 2. Fused beads and fibers at (a) low and (b) high concentration (M_w = 393,400 g/mol). The corresponding solution concentrations are indicated.

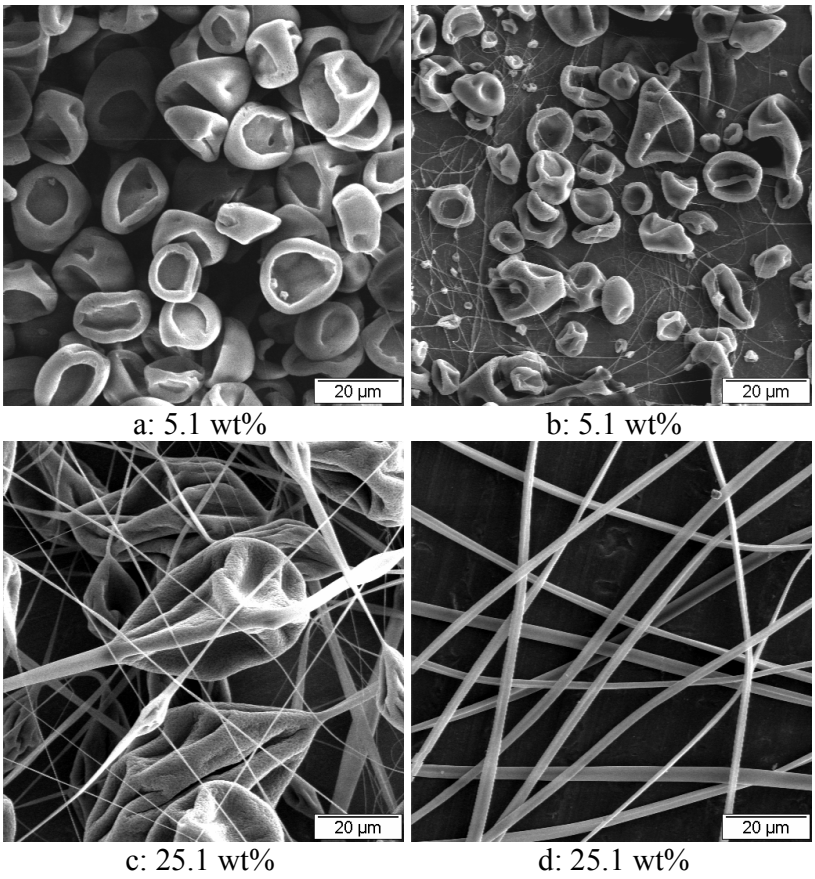

a: 5.1 wt% b: 5.1 wt%

c: 25.1 wt% d: 25.1 wt%

Fig. 3. SEM photographs showing the change in bead and fiber morphology with respect to applied voltage. Upon increasing the voltage from 10 kV (a, c) to 30 kV (b, d), fiber formation is facilitated. The corresponding solution concentrations are indicated (M_w = 111,400 g/mol).

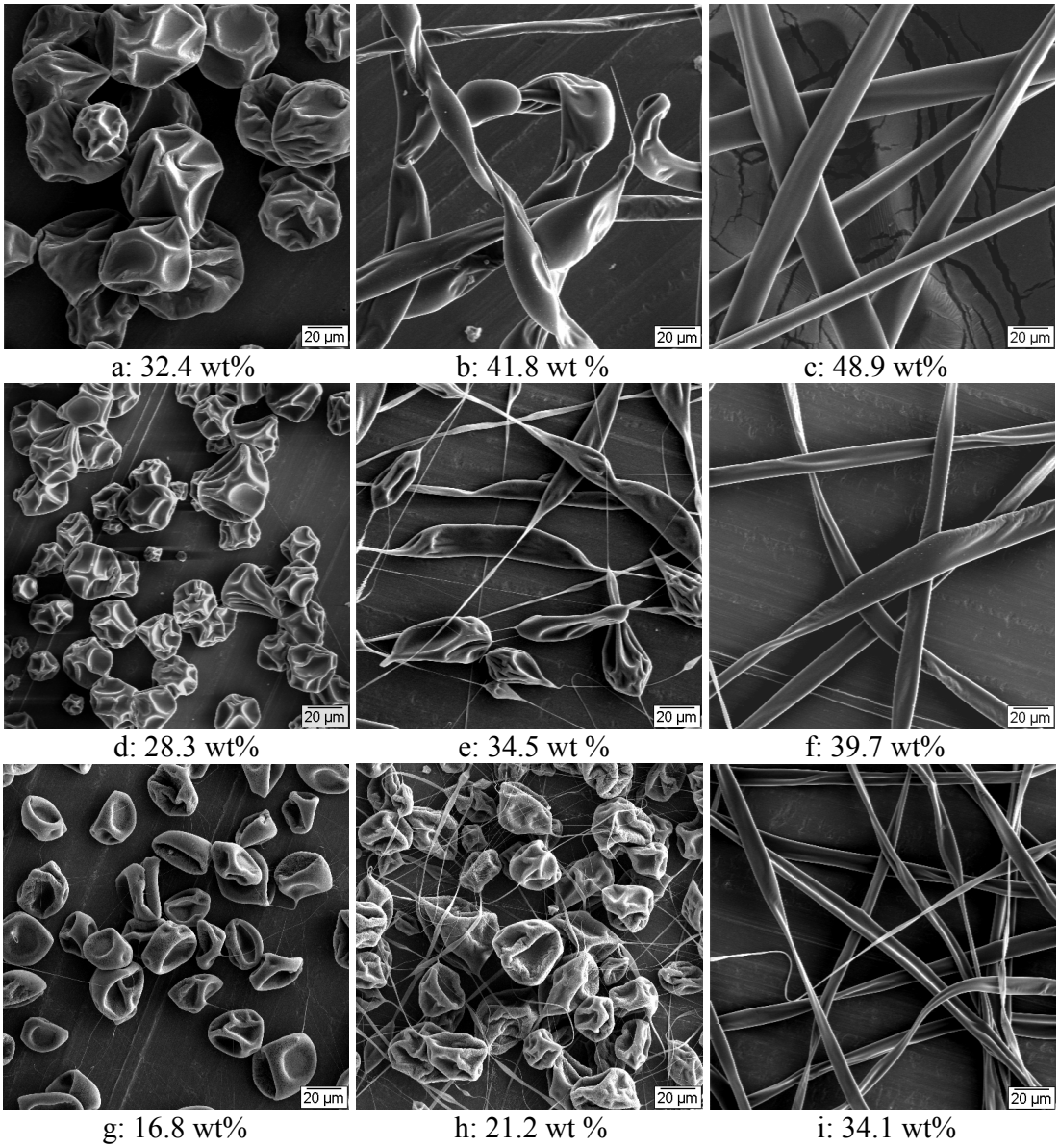

Figure 4. Bead to fiber transition observed with low to moderate molecular weight polystyrene ((a, b, c): M_w = 19,300 g/mol, (d, e, f): M_w = 44,100 g/mol, (g, h, i): M_w = 111,400 g/mol) electrospun from THF. The corresponding solution concentrations are indicated.

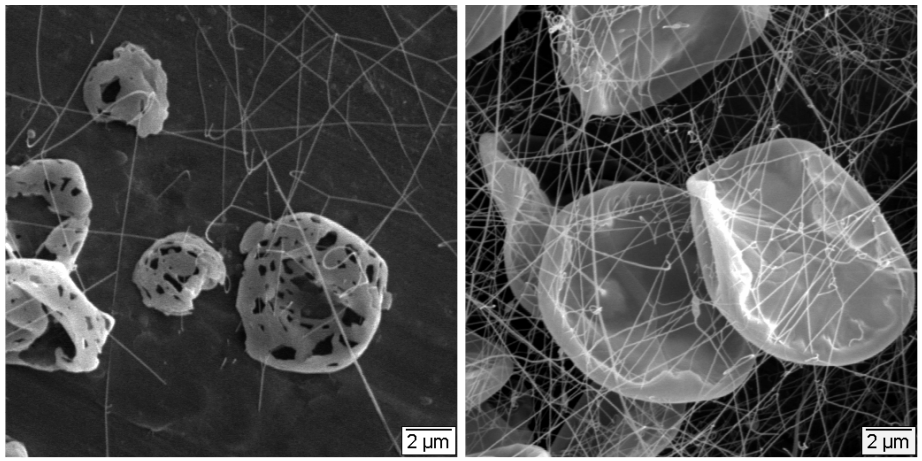

a: 0.11 wt% b: 0.34 wt%

Figure 5. Incipient fibers forming at extremely low concentrations for M_w = 1,877,000 g/mol ((a): C = 0.11 wt%, (b): C = 0.34 wt%)

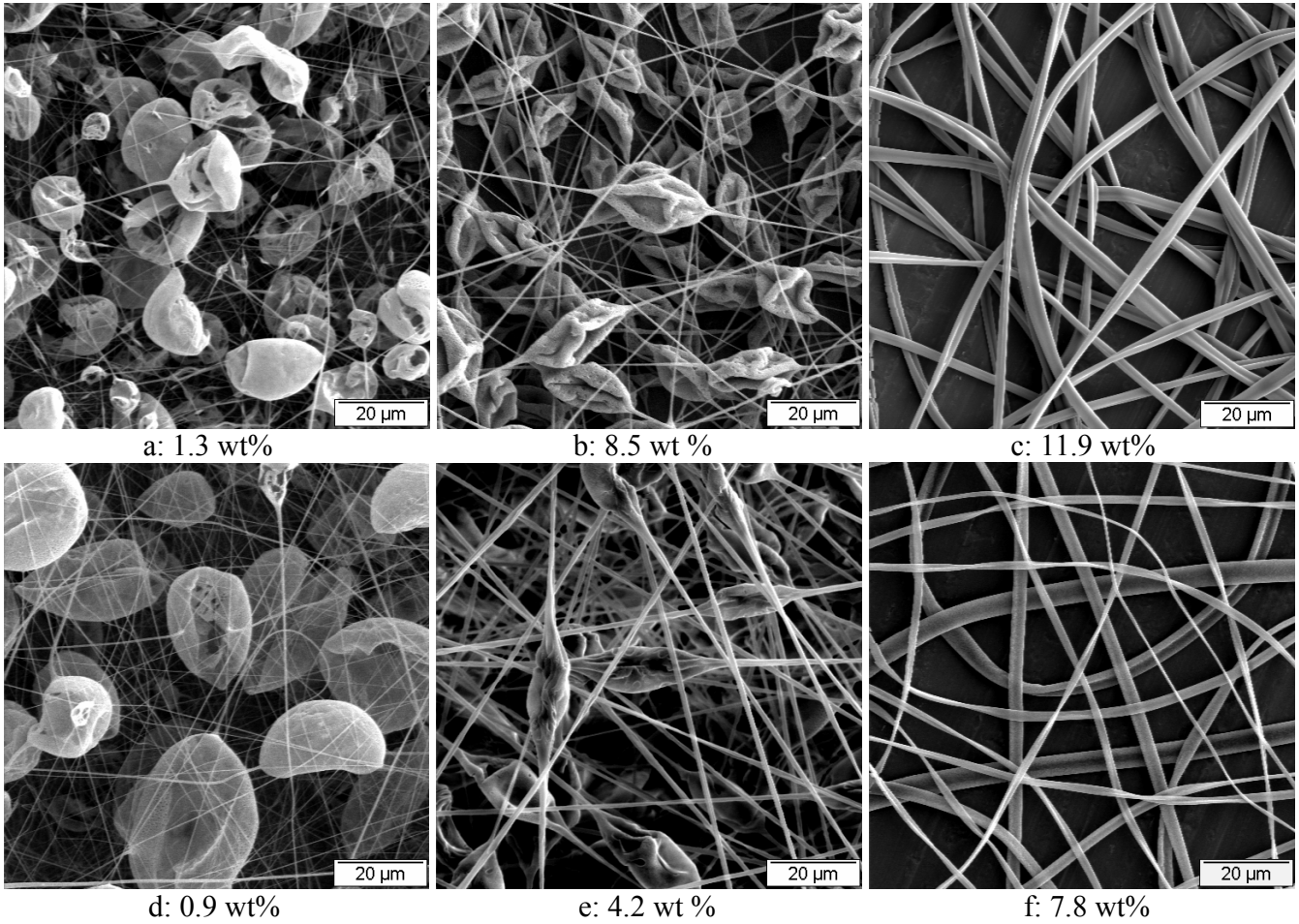

a: 1.3 wt% b: 8.5 wt % c: 11.9 wt%

d: 0.9 wt% e: 4.2 wt % f: 7.8 wt%

Figure 6. Change in the morphology of high molecular weight polystyrene ((a, b, c): 1,045,000 g/mol, (d, e, f): 1,877,000 g/mol) electrospun from THF. The corresponding solution concentrations are indicated.

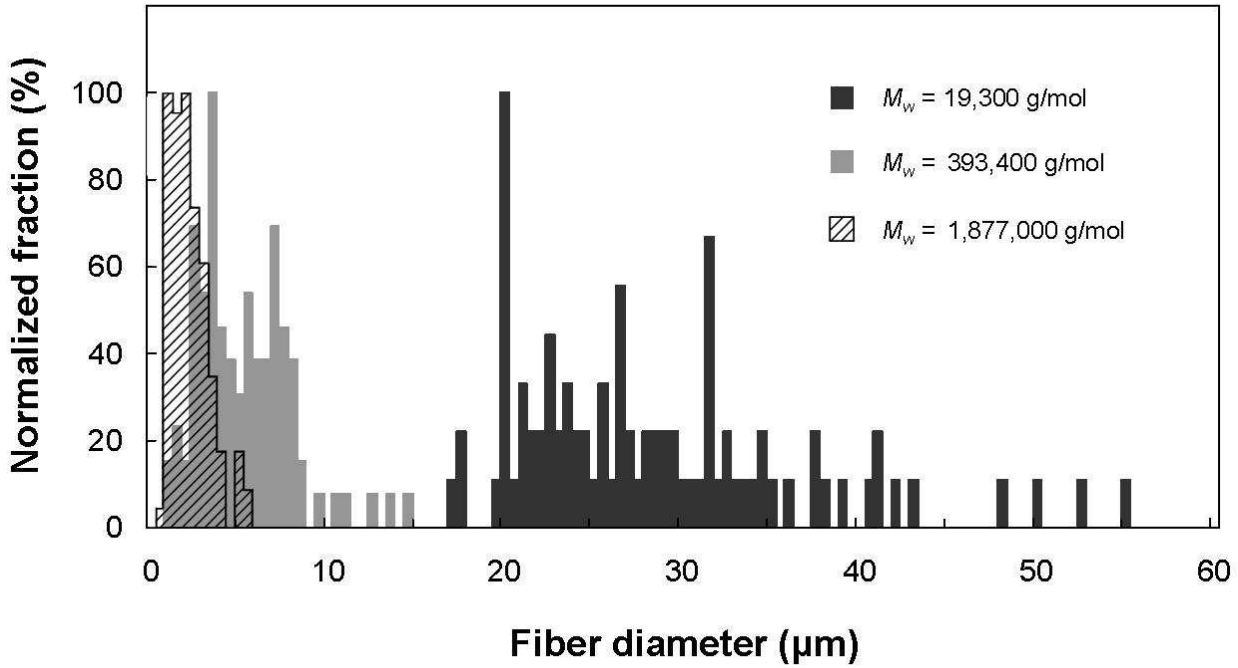

Figure 7. Fiber diameter distribution as a function of polymer molecular weight (M_w) at the critical concentration, C_f, at which bead-free fibers are observed for PS-THF system.

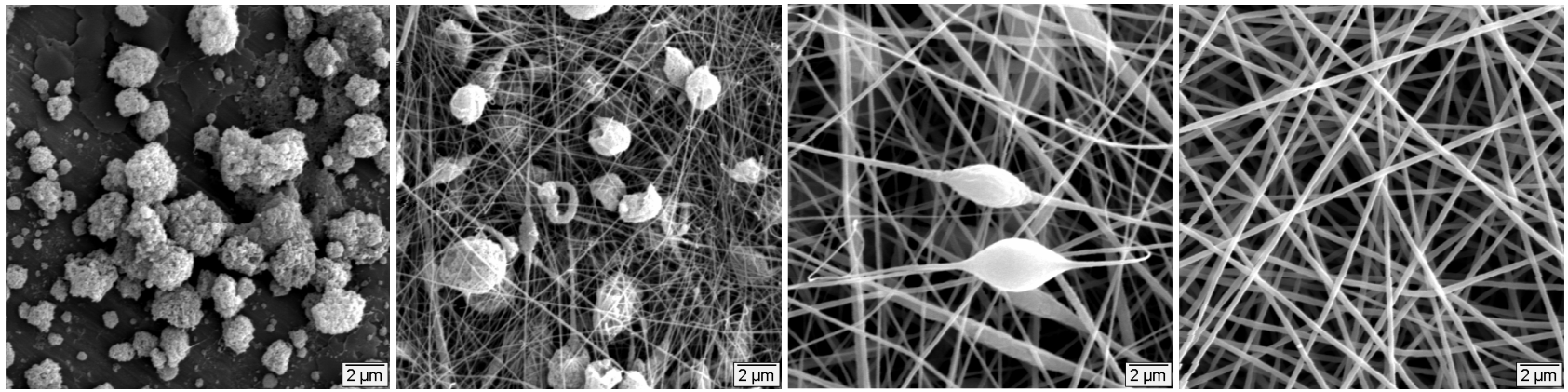

a: 2.5 wt% b: 4.8 wt% c: 13.1 wt% d: 20.2 wt%

Figure 8. Different structural regimes during bead-fiber transition of polystyrene electrospun from DMF. As the concentration is increased, the morphology consists of (a) beads only, (b) beads with incipient fibers, (c) bead-on-string, and (d) bead-free fibers. The corresponding solution concentrations are indicated.

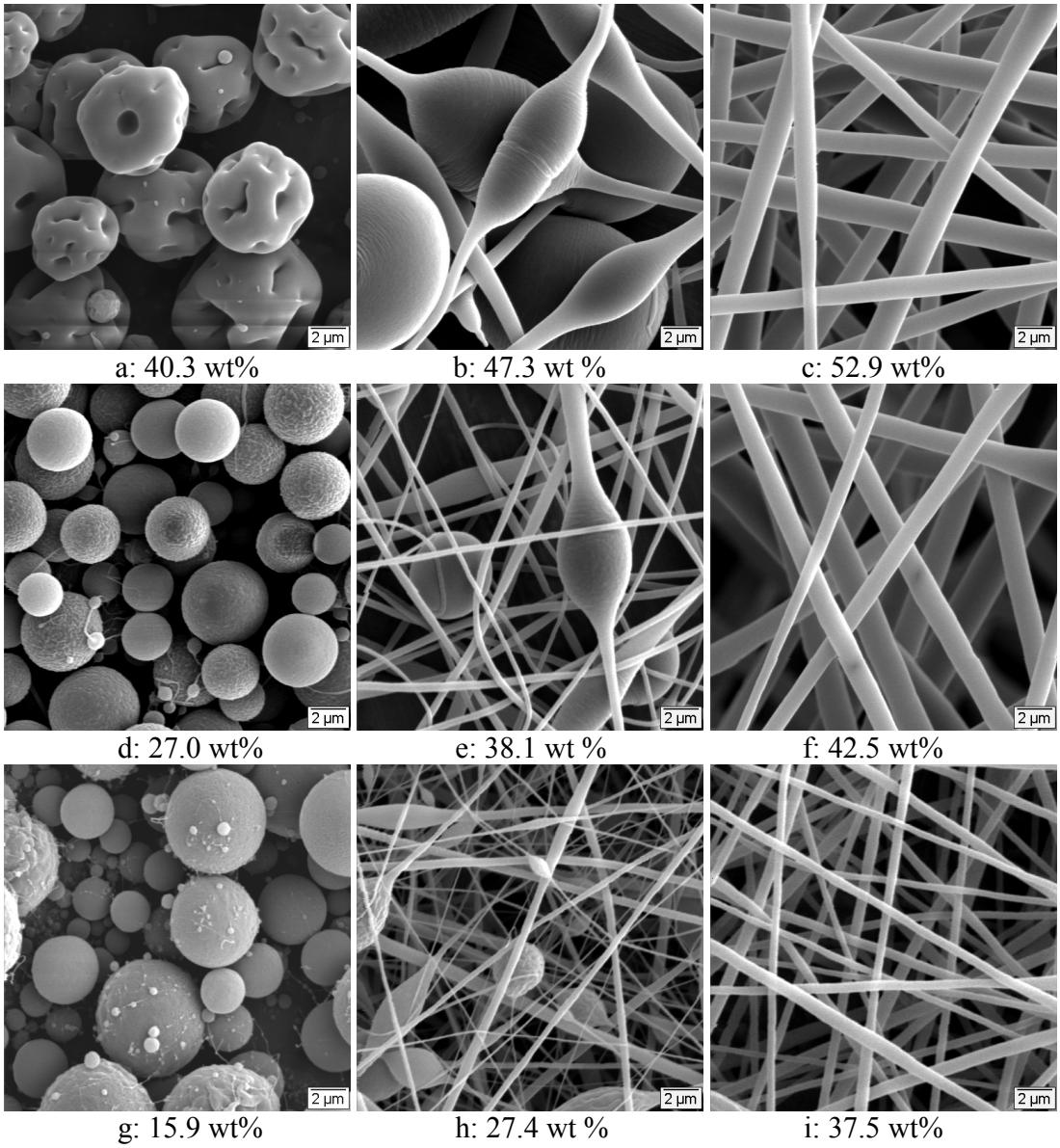

Figure 9. Bead-to-fiber transition observed with low to moderate molecular weight polystyrene ((a, b, c): 19,300 g/mol, (d, e, f): 44,100 g/mol, (g, h, i): 111,400 g/mol) electrospun from DMF. The corresponding solution concentrations are indicated.

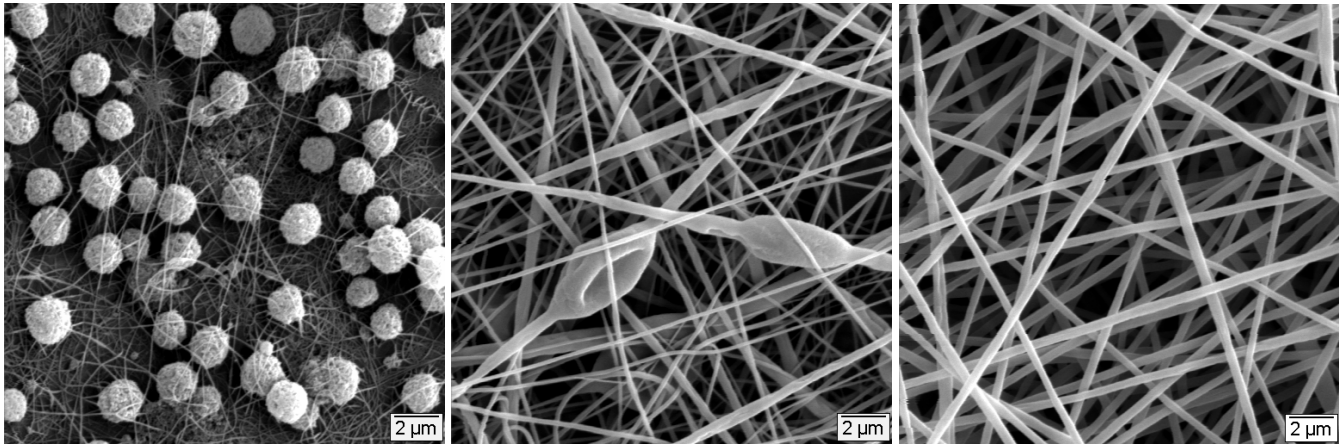

a: 1.3 wt% b: 7.0 wt % c: 11.2 wt%

d: 0.3 wt% e: 0.8 wt % f: 2.4 wt%

Figure 10. Change in the morphology of high molecular weight polystyrene ((a, b, c): 1,045,000 g/mol, (d, e, f): 1,877,000 g/mol) electrospun from DMF. The corresponding solution concentrations are indicated.

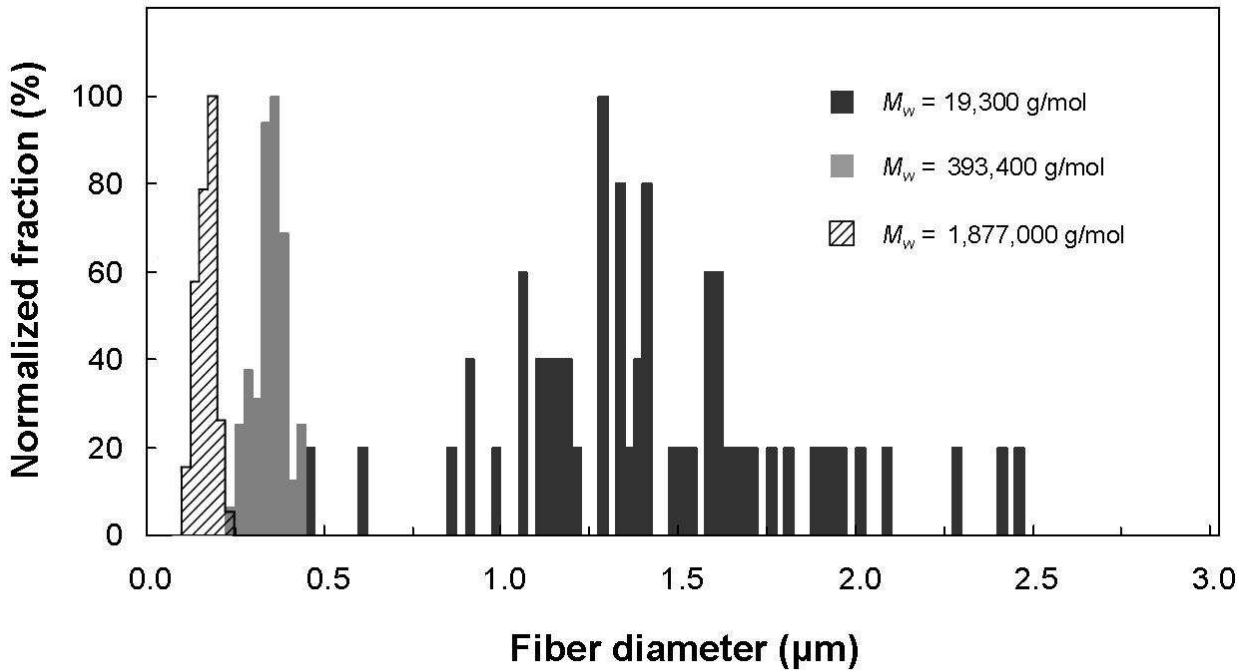

Figure 11. Fiber diameter distribution as a function of polymer molecular weight (M_w) at the critical concentration, C_f, at which bead-free fibers are observed for PS-DMF system.

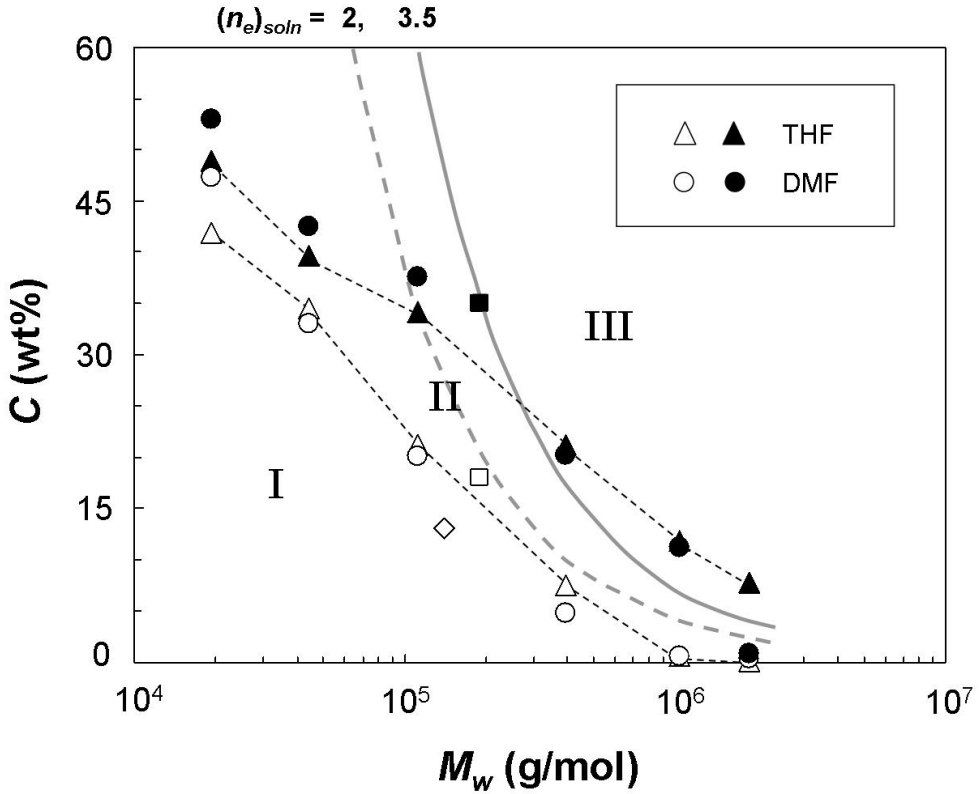

Figure 12. Variation of C_i and C_f as a function of molecular weight for PS-THF and PS-DMF systems. The regions I, II, and III indicate the conditions at which beads only, beaded fibers and bead-free fibers were observed respectively. The transition concentrations predicted from the solution entanglement number model [15] is plotted for comparison. The dashed and solid lines in gray indicate conditions corresponding to $(n_e)_{soln}$ = 2 and 3.5 respectively. The data of Megelski et al. (□,■) [10] and Lee et al. (◊) [20] are also shown. □ and ◊ indicate the conditions at which bead dominant morphologies are observed, whereas ■ corresponds to a condition at which bead-free fibers are observed.

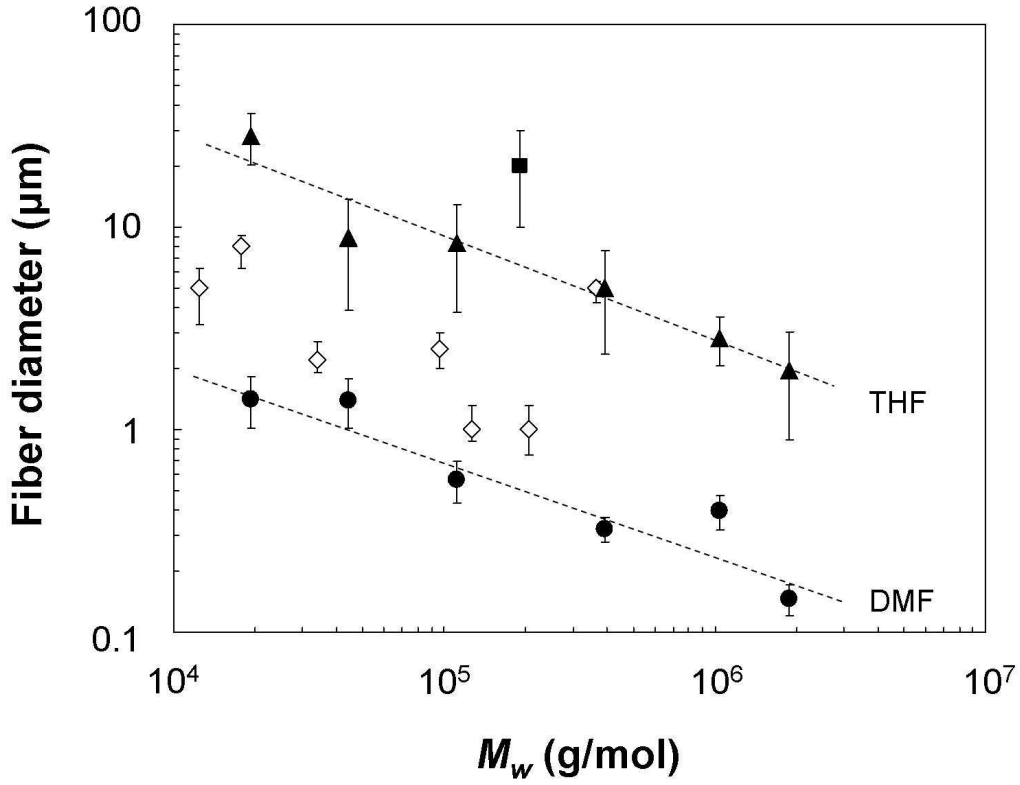

Figure 13. Average fiber diameter as a function of molecular weight for PS-THF and PS-DMF systems at the critical concentration, C_f, at which bead-free fibers are observed. The data of Megelski et al.[10] is indicated as a solid square (■). Relevant data of Gupta et al. [14], who examined PMMA-DMF system, are shown (as open diamond (◊)) for comparison.

Chapter 3

Solvent Effects on Jet Evolution during Electrospinning of Semi-dilute Polystyrene Solutions

Paper submitted for publication in *European Polymer Journal*, 2006

Paper submitted for publication in *European Polymer Journal*, 2006

Solvent Effects on Jet Evolution during Electrospinning of Semi-dilute Polystyrene Solutions

Goki Eda, James Liu, Satya Shivkumar*

Materials Science and Engineering Program,
Department of Mechanical Engineering,
Worcester Polytechnic Institute,
100 Institute Road,
Worcester, MA 01609

Abstract

Linear polystyrene with a weight average molecular weight of 393,400 g/mol was used with various solvents including tetrahydrofuran (THF), chloroform, carbon disulfide (CS_2), 1-methyl-2-pyrrolidinone (NMP), and N,N-dimethylformamide (DMF) to produce solutions, corresponding to a Berry number of about 9. The jet breakdown behavior of each of these solutions was studied with a high speed camera (2000 frames/s). The structure of the electrospun polymer was examined with a scanning electron microscope. The results indicate that jet breakdown with THF and chloroform entailed significant extensional flow, followed by the onset of instabilities, leading to the formation of numerous secondary jets under steady-state conditions. By comparison, the solution jets with DMF and NMP exhibit extensive whipping and splaying to produce a cloud of jets. In this case, few secondary jets were observed under steady-state conditions. A highly refined structure was observed in the electrospun polymer for NMP and DMF, in accordance with the extensive instabilties observed during jet breakdown. Limited jet instability observed with CS_2 solution suggests the significant effect of solvent evaporation. Typical primary jet velocities were measured to be on the order of 2-5 m/s.

Keywords: Polymer; Polystyrene; Electrospinning; Solvents

**Tel.:* +1 508 831 5048; *fax:* +1 508 831 5178
E-mail address: shivkuma@wpi.edu

Introduction

During electrospinning, various physical phenomena occur as the electrostatically driven jet of polymer solution travels across the electric field established between the capillary and the target. This process is initiated as a jet of solution breaks out of the conically protruded pendant drop known as the Taylor cone [1]. The ejected viscoelastic jet is driven towards the target, undergoing extensional flow. Subsequently, a repulsive Coulombic force in the jet results in bending instability and causes lateral perturbations to grow [2]. A high repulsive force in a thin jet may also cause splaying or splitting, resulting in further thinning of the jet [3,4]. Micro- to nanometer scale fibers and beads of various morphologies may be produced as a consequence of repeated jet thinning. The principal features of this process have been summarized in a recent review [5].

The structures produced during electrospinning can consist of beads, fibers, or a combination of the two, often referred to as bead-on-string structures [6,7]. Several investigators have shown that a bead to fiber transition may occur as the molecular weight and/or the concentration of the polymer in solution is increased [8-10]. Stable fibers may be produced when sufficient chain entanglements are present in the solution [10,11].

The overall morphology of the electrospun polymer is strongly influenced by the physical and electrical properties of the solution, determined to a large extent by the type of solvent [7,12]. For example, it has been reported that solvents with high dielectric constant typically result in finer and more uniform fibers in the electrospun polymer [12-16]. The development of

the structure in the polymer obtained on the collector and the corresponding role of the solvent has not been clearly understood. Koombhongse et al. [4] have shown that jet instabilities developing at the Taylor cone may be influenced by the type of solvent used for the spinning process. Their results indicate that the characteristics of the fibers in the structure obtained on the collector may depend on the extent of bending instability, splaying and splitting. The development of these jet instabilities is a complex phenomenon that is controlled by several factors including solution rheology, charge density, surface tension and solvent evaporation rate [17,18]. Since the morphology of electrospun fibers may depend on various solvent properties, the jet breakdown behavior may be unique to a specific polymer-solvent system. The purpose of this work is to study the jet evolution with polystyrene with various solvents by utilizing a high speed camera. Experiments have been conducted with moderate to good solvents, with widely varying dielectric constant and evaporation rates.

Experimental procedure

Linear polystyrene with a weight average molecular weight (M_w) of 393,400 g/mol and polydispersity of 1.16 (Scientific Polymer Products, Ontario, NY) was dissolved in various solvents (reagent grade) shown in Table 1. The concentration of polymer was adjusted such that the Berry number, $[\eta]C$, was around 9 ($[\eta]$ is the intrinsic viscosity and C is the concentration) [19]. The concentration was calculated according to:

$$C(\text{g/mol}) = \frac{9}{[\eta]} = \frac{9}{KM_w^a} \qquad (1)$$

where K and a are the Mark-Houwink constants based on the polymer, solvent and temperature [20]. The values of K and a for different solvents are listed in Table 2 [21-23]. The Mark-Houwink constants for most of the solvents used in this study were readily available for most solvents, typically obtainable from many sources. These constants (Table 2) were used in eqn (1) to calculate the concentration of the polymer. The Mark-Houwink constants for the polystyrene-CS_2 system, however, were not readily available. Consequently, experiments with CS_2 were conducted at the same concentration as that of THF (Table 2). Based on the only available source for the Mark-Houwink constant for this system [23], the approximate $[\eta]C$ for this condition was calculated to be 7.5. It should be noted that CS_2 was selected as solvent because of its extremely high vaporization rate compared to the other solvents used in the study. Approximately 0.04~0.06 g of polymer was dissolved in 0.5 mL of solvent to achieve the desired solution concentration (Table 2). The solution was obtained in a 1 mL syringe equipped with an 18 gauge needle (Inner diameter = 0.84 mm, 51 mm long). The syringe was placed horizontally on a syringe pump (EW-74900-00, Cole-Parmer) as shown in Fig. 1. A grounded aluminum foil collector (10 cm×10 cm) was positioned 10 cm from the tip of the needle. The pump was calibrated to achieve a flow rate of 3 mL/hr for all experiments. A potential of 30 kV was applied to the needle immediately after a pendant drop formed at the tip. A high speed camera (Phantom V.5.1., Vision Research) equipped with Nikon 150 mm lens was used to capture the solution jet images at a rate of 2000 frames per second with exposure time of 259 μs. The images were extracted and analyzed using the proprietary software (CineView606) supplied by Vision Research. The morphology of the electrospun fibers was examined with a scanning electron microscope (JSM-840) after sputter-coating the sample with gold-palladium.

Results and Discussion

The rheology of polymer solutions has a significant effect on the morphology of electrospun fibers [10,24,25]. The interaction of polymer molecules in solution can be described in terms of C^*, the dilute solution limit at which the hydrodynamic volumes of the dissolved molecules begin to overlap, and C_e, the entanglement concentration [10]. The concentration C_e can be considered to be a crossover from a concentration range where intramolecular excluded-volume effects control the solution viscosity to a regime where intermolecular entanglements begin to have a significant effect on the rheological properties of the solution. When the concentration is increased beyond C_e, the zero shear viscosity shows a steep increase due to the extensive entanglements of the polymer chains. It has been reported that during electrospinning, stable fibers can be formed with solutions in this regime *i.e.* $C > C_e$ [10]. Shenoy et al. [11] proposed that the transition from bead-only to a bead-on-string structure occurs at a concentration corresponding to one entanglement per chain. The degree of chain overlap can also be expressed in terms of the Berry number, $[\eta]C$ [19]. For polystyrene with a M_w = 390,000 g/ml in a good solvent such as tetrahydrofuran (THF), C_e has been measured to be around 0.06 g/ml [26], which corresponds to $[\eta]C$ value of 7.8. Lee et al. [27] have electrospun polystyrene with THF as the solvent for a solution concentration equivalent to $[\eta]C$ of about 8. The morphology consisted of beaded fibers and half hollow spheres. Megelski et al. [9] have produced polystyrene fibers with THF as the solvent for a range of concentration equivalent to $[\eta]C$ of 14 to 35. They obtained a bead-on-string structure at $[\eta]C$ of 14 and a fully fibrous structure at $[\eta]C$ of 35. These results suggest that there is a general agreement with the theory in terms of entanglement concentration and fiber formation. For polystyrene-THF system in this

study, the minimum concentration at which some stable fibers were observed corresponded to $[\eta]C$ of 9.

Photographs showing the structure in the electrospun polymer are shown in Fig. 2 for various solvents used in this study. When THF, chloroform, or carbon disulfide (CS_2) were used as solvents, the structure consisted of fine fibers, cups and dimpled beads, typically on the order of 10 to 20 μm, similar to the data of Lee et al. [27]. The morphology obtained with 1-methyl-2-pyrrolidinone (NMP) solution consisted of a number of beads, which were much smaller in size (1~5 μm) compared to those obtained with THF, chloroform, and CS_2 (Fig. 2(d)). Some fibers connecting these beads were also observed indicating that the solution concentration was in the transition regime. The fine structure obtained with NMP implies the high charge density achieved resulting from repeated breakdown of solution jet. In contrast to these bead dominant morphologies, a highly fibrous structure was obtained with N,N-dimethylformamide (DMF) solution indicating that the transition from bead to fiber may occur with smaller degree of chain overlap (Fig. 2(e)).

Various stages in the development of the jet as the solution emerges from the capillary are shown in Fig. 3 for THF. The ejected jet of solution underwent an extensional flow for the first few milliseconds after jet initiation and traveled in a straight line for a distance of about 25 mm from the capillary. Subsequently, about 7 ms after jet initiation, the tip of the jet broke down into a number of beads, which are seen as bright segments in Fig. 3. The beads are seen as bright segments due to their high velocity. The formation of beads indicates insufficient chain entanglement. However, because the solution concentration is in the entanglement regime, it can

be expected that these beads may be connected by thin fibers that are not visible in the photograph. It is likely that bead formation was triggered by bending instability at the tip of the jet. About 11 ms after jet initiation, small perturbations along the jet became large, yielding a wave-like profile (Fig. 3). The perturbation indicated by the arrow in Fig. 3 gradually grew into the bent jets shown in Fig. 4. This bending may have been caused not only by the electrical force but also by the buckling in the segment. In this case, the compressive force may have resulted because the thick segment of the jet (indicated by the arrow in Fig. 3) advanced relatively slowly compared to the fresh jet ejected from the capillary. The arrow in Fig. 4 indicates the looping of the jet, which was observed in more detail with back scattered lighting as shown in Fig. 5(a). This loop of jet eventually breaks down into beads as discussed above. The back scattered photographs show that as the jet of THF solution flowed out of the initial drop, the surface of the Taylor cone receded to the capillary tip. Subsequently, a secondary jet appeared from the edge of the capillary as shown in Fig. 5(b). This secondary jet was observed typically 20 to 30 ms after primary jet initiation. The bending instability of the primary jet became less intensive after the emergence of the secondary jet and, subsequently, these jets essentially became indistinguishable (Figs. 5(b) and (c)). Several jets appeared in a similar fashion from the capillary end one after another until a pseudo-steady state was reached (Fig. 6). At this stage, the Taylor cone was no longer observable suggesting that it had moved inside the capillary, as has been reported previously [6,28]. Numerous steady-state minijets were ejected in the radial direction from the edge of the capillary. It is likely that these minijets were ejected towards the direction where the electric field was the strongest. The development of bending instability at the end of each of the minijets can also be seen in Fig. 6 (similar to the looping in the secondary jet observed in Fig. 5(c)). A photograph of the needle tip after electrospinning, highlighting

solidified fibers is shown in Fig. 7. The direction of the solidified fibers matches the profile observed during steady-state flow (Fig. 6). The photograph shown in Fig. 7 also indicates the complex nature of jet instability.

A similar trend in jet evolution was observed when chloroform was used as the solvent as shown in Fig. 8. The primary jet underwent elongational flow for the initial few milliseconds after it emerged from the Taylor cone. Bending instability was observed in both the primary and the secondary jet, as was the case for THF solution. The perturbations in the primary jet grew considerably and eventually enabled the jet to break down into beads in a manner similar to that observed with THF solution (Fig. 8(c)). As the Taylor cone receded to the capillary, secondary jets were ejected one after another from the edge of the capillary until a steady-state profile was observed (Fig. 8(d)). This steady-state was reached about 40 ms after jet initiation.

The jet breakdown observed with DMF as the solvent was significantly different from either THF or chloroform. In this case, a jet of solution was ejected from the Taylor cone and immediately formed a cloud of jet a few millimeters away from the Taylor cone as shown in Fig. 9. This cloud may consist of jets undergoing splaying and whipping at a high frequency. The lateral size of the cloud grew for a few milliseconds and remained constant about 8 ms after jet initiation. The breakup of the jet indicates that the electrical force due to the charges in the jet became large enough to overcome the surface tension and the viscoelastic force of the solution. It can be expected that the relatively high dielectric constant and the polyelectrolyte behavior of DMF may promote a high charge density in the jet. A similar discussion about the effect of DMF has been reported previously [10-15]. The surface tension of DMF is slightly larger than

that of THF or chloroform, which implies that a larger force is required to cause bending and splaying. The immediate breakup of the jet, therefore, suggests that the charge density within the jet of DMF solution was significantly higher than that in THF and chloroform solution. As the jet progressed, an oscillation was observed in the cloud of jet (Fig. 9). The oscillation of the cloud eventually evolved into a spiral, in a manner much similar to the development of bending instability of a single jet. This phenomenon was reported by Reneker et al. [29] for polycaprolactone in acetone. Reneker et al. [29] measured the length of the straight segment of the jet before the onset of instability to be around 3 mm, which is comparable to the value obtained in this study with DMF solution (although the electric field strengths are different in these experiments). During jet evolution, a change in the shape of the Taylor cone was often observed as shown in Fig. 9. This change may be due to the balancing of the excess charge accumulated in the Taylor cone and the charge that is dispensed together with the jet. It was often observed that when the Taylor cone was in a conical shape, the breakup of the jet was more significant and occurred closer to the Taylor cone, suggesting a variation of charge density within the jet.

The jet of DMF solution underwent a series of chaotic events before reaching a steady state. Sequential photographs demonstrating secondary jet development and the chaotic events in these jets are shown in Fig. 10. The secondary jet appeared and developed a whipping motion in a similar fashion as the primary jet. During the secondary jet formation, the vertex of the Taylor cone directed towards the emerging secondary jet, suggesting the inequality in the charges distributed to the two jets. The Taylor cone returned to the unperturbed hemispherical shape after the secondary jet stabilized. After the formation of the secondary jet, Taylor cone

became elongated and went through a whipping motion which resulted in the detachment of the two jets (Fig. 10). After this event, the primary jet formation was started over. The jets that formed at this stage were extremely unstable and showed extensive whipping as seen in the lower jet (indicated by the arrow) in Fig. 11. These instabilities continued for about 100 ms and eventually, a steady-state profile was reached as shown in Fig. 12. Unlike the case of THF and chloroform, the Taylor cone is still observable at this stage with DMF solution. Five steady-state jets can be seen to break down into clouds of jet approximately equal distance from the capillary tip. The lateral sizes of the jet cloud are also approximately equal.

The jet evolution observed with NMP as the solvent showed a trend similar to that of DMF solution. The ejected jet of NMP solution immediately broke down into a cloud of jet as shown in Fig. 13. Splaying of jet was frequently observed for a few milliseconds after the formation of a jet. The occurrence of the splaying coincided with the meniscus attaining a conical shape as opposed to hemispherical shape, indicating the presence of high excess charge within the Taylor cone. The lateral size of the cloud grew larger and more diffuse compared to DMF solutions suggesting that the jet broke down into a number of beads as was observed in the microstructure (Fig. 2). Subsequently various unstable events were observed and continued until a steady-state was reached. Elongation and whipping of the Taylor cone and a merging of the primary and the secondary jet were frequently observed in this stage (Fig. 13). The steady-state profile was reached typically about 160 ms after jet initiation. The Taylor cone was observed outside the capillary at this stage. Fig. 14 shows five jets breaking down into a cloud of jets. The cloud of jets did not exhibit a whipping motion unlike the DMF solution, suggesting highly dispersed charges in the space.

The jet evolution with CS_2 as the solvent showed a different behavior compared to the previous solvents, as shown in Fig. 15. After the formation of the Taylor cone, small droplets were ejected from the vertex. While the droplets were ejected, the Taylor cone was stretched towards the collector and Rayleigh instability caused this elongated Taylor cone to break into droplets. This breakup continued until a fresh Taylor cone was formed and a stable jet was ejected. This late formation and the singularity of the stable jet is possibly due to the extremely low boiling point of CS_2, which may have resulted in the formation of skin on the surface of the initial Taylor cone. The stable jet exhibited some degree of instability as indicated by the arrow in Fig. 15, however, it remained as a single straight jet most of the time. After about 40 ms of steady jet observation, the Taylor cone began to stretch as in the preliminary stage of jet formation and this process was repeated.

The transient jet velocity of each solution immediately after jet initiation was measured. In each frame following jet initiation, position of the jet was recorded by marking the tip of the jet. In the case of DMF and NMP solution, the position at the tip of the jet cloud was recorded. The average velocity of the jet between two successive frames was thus calculated for each solution. The variation of the jet velocity with the time elapsed after jet initiation is plotted in Fig. 16. The jet velocity of THF, chloroform, and CS_2 solution was found to be relatively constant during the observed time interval. The constant jet velocity suggests that equilibrium is established between the electrical force pulling the jet towards the collector and the resisting viscoelastic force. On the other hand, DMF and NMP solutions exhibited a dramatic decrease in velocity in the first 2 ms after jet initiation. This deceleration coincides with the jet breakup,

which DMF and NMP solutions undergo immediately after jet initiation (Figs. 9 and 13). The complex trajectory within the jet cloud may have resulted in the reduction of velocity. The velocity of the jet reported by Reneker et al. [29] for the polycaprolactone-acetone system is about 0.7 m/s. By comparison, steady-state primary jet velocities in this study were generally between 2 to 5 m/s (Fig. 16).

It was observed that the overall jet evolution and breakdown can be grouped into two categories as shown in Fig. 17. The jet evolution observed with the first group of solvents, THF and chloroform, can be characterized by high degree of extensional flow, limited instability, and a large number of secondary jets. The jet evolution of this group of solvents involved a large bending of the primary jet, followed by the emergence of the secondary jets. On the other hand, DMF and NMP solutions exhibited a limited extensional flow, high degree of instability, and a small number of secondary jets. CS_2 was not included in either of the categories. The various instability phenomena observed with DMF and NMP suggest that the electric properties of the solution play a dominant role in structure formation.

Bending instability of an electrified jet causes small perturbations along the jet to grow as they travel towards the collector. Because the position at which this perturbation starts to grow and its growth rate are relatively constant for a given condition, a jet of solution undergoing bending instability typically produces a shape referred to as an envelope cone [18]. The shape and the size of the envelope cone are determined by various factors such as the initial charge density, surface tension and the viscoelastic properties of the solution. The observation of envelope cone shape is important because it is related to the draw ratio of the jet, as has been

described by Yarin et al. [18]. In this experiment, a stable cone was observed for all the solutions except for CS_2. In these solutions, a stable cone was observed in the early stage of the primary jet development and in secondary jets. The size of the envelope cone was measured from photographs in which a stable cone could be observed. An example of this envelope cone is shown in Fig. 3. The jet breaks into a number of beads, which together form a cone shape with its vertex lying at the end of the extensional flow. The radius of the cone was measured and plotted as a function of the distance from the capillary tip as shown in Fig. 18. It is clearly seen that the development of instability is much more rapid and occurs earlier for DMF and NMP solutions compared to THF and chloroform solutions. This trend is observed for both the primary and the secondary jets indicating the presence of high charge density in these jets. The reasons for the differences observed in the envelope cone shape between the DMF and NMP solution are not readily evident; however, it is likely that the NMP solution did not have sufficient viscosity and broke down into beads immediately after the initial whipping of jet as speculated from the microstructure (Fig. 2). Another factor determining the envelope cone shape is the evaporation of the solvent. Yarin et al. [18] theoretically determined the radius of the envelope cone and found that when the evaporation of the solvent is not taken into account in the calculation, the radius of the envelope cone grew more rapidly compared to their experimental data. As evaporation and solidification take place, viscosity and elastic modulus of the jet increase dramatically, leading to a slow stretching of the jet. The fact that no stable cone was formed with CS_2 implies that the effect of evaporation was significant. An increased jet stiffness resulting from rapid solidification may have suppressed bending instability. However, solvent evaporation rate and electrical properties should not be considered independently because instability phenomena increase the jet surface area where solvent can evaporate.

Conclusions

Solvents used for electrospinning have a major effect on the various physical phenomena occurring during the formation and disintegration of the jets emerging from the Taylor cone. For solutions in the transition regime between beads and beaded fibers, two classes of solvents were identified. The first class of solvents is characterized by large extensional flow, limited degree of instability, and a large number of the secondary jets that form under steady-state conditions. In this case, the primary jet velocity is relatively constant (3 to 4 m/s). THF and chloroform are examples of this type of behavior. In solvents with a high dielectric constant such as DMF and NMP, the jet breakdown occurs through repeated whipping and splaying to produce a cloud of jets. In this case, there was a reduction in jet velocity after the onset of bending and whipping instabilities. Steady-state velocities, however, were comparable to the value obtained with THF and chloroform. The rapid skin formation with highly volatile solvents such as CS_2 may inhibit the development of jet instabilities and thereby minimize the formation of secondary jets. The structure in the electrospun polymer was similar for THF, chloroform and CS_2 and consisted of fine fibers, cups and dimpled beads, typically on the order of 10 to 20 μm. In the case of DMF and NMP, the beads and fibers were highly refined (~1 to 5 μm) confirming the extensive instabilities the solution experiences during electrospinning.

References

[1] G.I. Taylor, Proc. Roy. Soc. Lond. A (1969) 313-453.
[2] D.H. Reneker, A.L. Yarin, H. Fong, S. Koombhongse, J. Appl. Phys. 87 (2000) 4531.
[3] D.H. Reneker, I. Chun, Nanotechnology, 7 (1996) 216-223.

[4] S. Koombhongse, W. Liu, D.H. Reneker, J. Polym. Sci., Part B: Polym. Phys. 39 (2001) 2598-2606.
[5] T. Subbiah, G.S. Bhat, R.W. Tock, S. Parameswaran, S.S. Ramkumar, J. Appl. Polym. Sci. 96 (2005) 557-569.
[6] J.M. Deitzel, J. Kleinmeyer, D. Harris, N.C.B. Tan, Polymer 42 (2001) 261-272.
[7] H. Fong, I. Chun, D.H. Reneker, Polymer 40 (1999) 4585-4592.
[8] X. Zong, K. Kim, D. Fang, S. Ran, B.S. Hsiao, B. Chu, Polymer 43 (2002) 4403-4412.
[9] S. Megelski, J.S. Stephens, J.F. Rabolt, D.B. Chase, Macromolecules, 35 (2002) 8456-8466.
[10] P. Gupta, C. Elkins, T.E. Long, G.L. Wilkes, Polymer 46 (2005) 4799-4810.
[11] S.L. Shenoy, W.D. Bates, H.L. Frisch, G.E. Wnek, Polymer 46 (2005) 3372-3384.
[12] W.K. Son, J.H. Youk, T.S. Lee, W.H. Park, Polymer 45 (2004) 2959-2966.
[13] K.H. Lee, H.Y. Kim, Y.M. La, D.R. Lee, N.H. Sung, J. Polym. Sci., Part B: Polym. Phys. 40 (2002) 2259-2268.
[14] K.H. Lee, H.Y. Kim, M.S. Khil, Y.M. Ra, D.R. Lee, Polymer 44 (2003) 1287-1294.
[15] C.M. Hsu, S. Shivkumar, Macromol. Mater. Eng. 289 (2004) 334-340.
[16] Q. Yang, L.I. Zhenyu, Y. Hong, Y. Zhao, S. Qiu, C.E. Wang, Y. Wei, J. Polym. Sci., Part B: Polym. Phys. 42 (2004) 3721-3726.
[17] M.M. Hohman, M. Shin, G. Rutledge, M.P. Brenner, Phys. Fluids 13 (2001) 2201-2220.
[18] A.L. Yarin, S. Koombhongse, D.H. Reneker, J. Appl. Phys. 90 (2001) 4836.
[19] B.L. Hager, G.C. Berry, J. Polym. Sci. Polym. Phys. Ed. 20 (1982) 911-928.
[20] L.H. Sperling. Introduction to Physical Polymer Science 2nd ed., Wiley, NewYork, 1992.
[21] J. Brandrup, E.H. Immergut, E.A. Grulke. Polymer Handbook 4th ed., Wiley, New York, 1999.
[22] J.M. Peureux, P. Lochon. European Polym. J. 19 (1983) 565-574.
[23] Y.S.J. Gan, R. Nuffer, J.M. Guenet, J. Francois, Polym. Commun. 27 (1986) 233-235.
[24] A. Koski., K. Yim, S. Shivkumar, Mater. Lett. 58 (2004) 493-497.
[25] M.G. McKee, G.L. Wilkes, R.H. Colby, T.E. Long, Macromolecules, 37 (2004) 1760-1767.
[26] A.M. Jamieson, D. Telford. Macromolecules 15 (1982) 1329.
[27] K.H. Lee, H.Y. Kim, H.J. Bang, Y.H. Jung, S.G. Lee, Polymer 44 (2003) 4029-4034.
[28] Y.M. Shin, M.M. Hohman, M.P. Brenner, G.C. Rutledge, Polymer 42 (2001) 9955-9967.
[29] D.H. Reneker, W. Kataphinan, A. Theron, E. Zussman, A.L. Yarin, Polymer 43 (2002) 6785-6794.
[30] J.A. Riddick, W.B. Bunger, T.K. Sakano, A. Weissberger, Organic solvents: physical properties and methods of purification, Techniques of chemistry vol. 2 4th ed., Wiley, New York, 1986.

Table 1 *Solvents used in this study. Relevant properties of the solvent including boiling point (bp), heat of vaporization (ΔH_v), dielectric constant (ε), viscosity (η) and surface tension (γ) are also shown [30].*

Solvent	Supplier	*bp* (°C)	ΔH_v (kJ·mol^{-1})	ε	$\eta \times 10^3$ (kg·m^{-1}·s^{-1})	$\gamma \times 10^2$ (N·m^{-1})
Tetrahydrofuran	Sigma-Aldrich	66	32.0	7.58	0.46	2.64
Chloroform	Alfa Aesar	61	33.3	4.81	0.536	2.653
N,N-Dimethylformamide	Sigma	153	47.5	36.71	0.802	3.642
1-Methyl-2-pyrrolidinone	Sigma-Aldrich	202	52.8	32.20	1.67	4.07
Carbon disulfide	Sigma-Aldrich	46	27.5	2.64	0.363	3.225

Table 2 *Mark-Houwink constants for the solvents used in this study. The temperature, T, at which the data have been reported, is indicated. The concentration of polymer used in the experiment (C), the intrinsic viscosity [η] and the corresponding Berry number ([η]C) are also shown. Polystyrene with a weight average molecular weight (M_w) of 393,400 g/mol was used in all the experiments.*

Solvent	$K \times 10^3$ (mL/g)	*a*	*T* (°C)	Reference	*C* (g/mL)	[η] (mL/g)	[η]*C*
Tetrahydrofuran	11	0.725	25	[21]	0.072	125	9.0
Chloroform	7.16	0.76	25	[21]	0.070	128	8.9
N,N-Dimethylformamide	31.8	0.603	35	[21]	0.120	75	9.0
1-Methyl-2-pyrrolidinone	12	0.72	85	[22]	0.071	128	9.2
Carbon disulfide	3.46	0.8	25	[23]	0.072	104	7.5

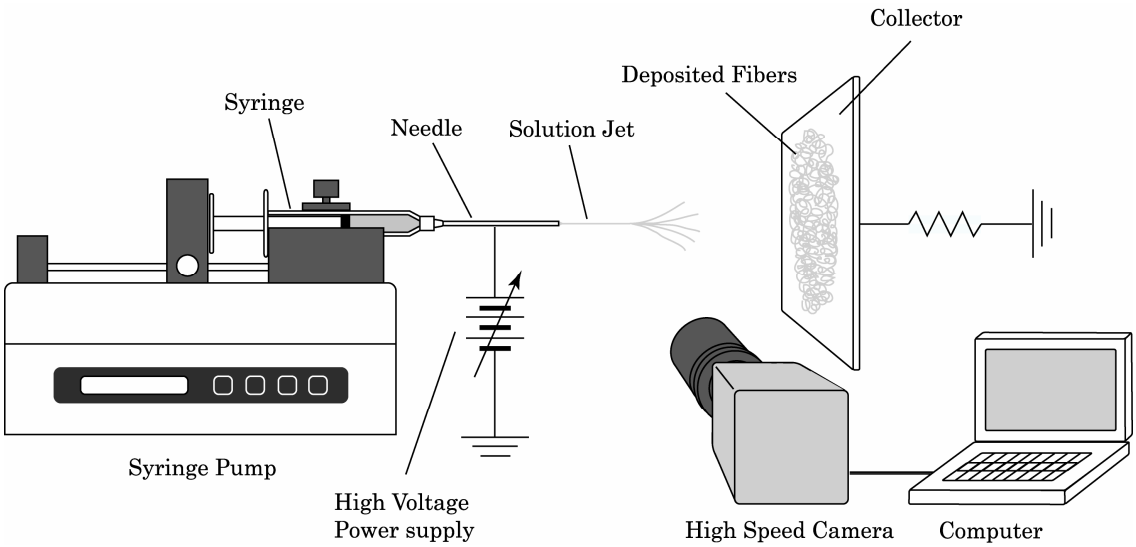

Fig. 1. Schematic of the experimental set-up.

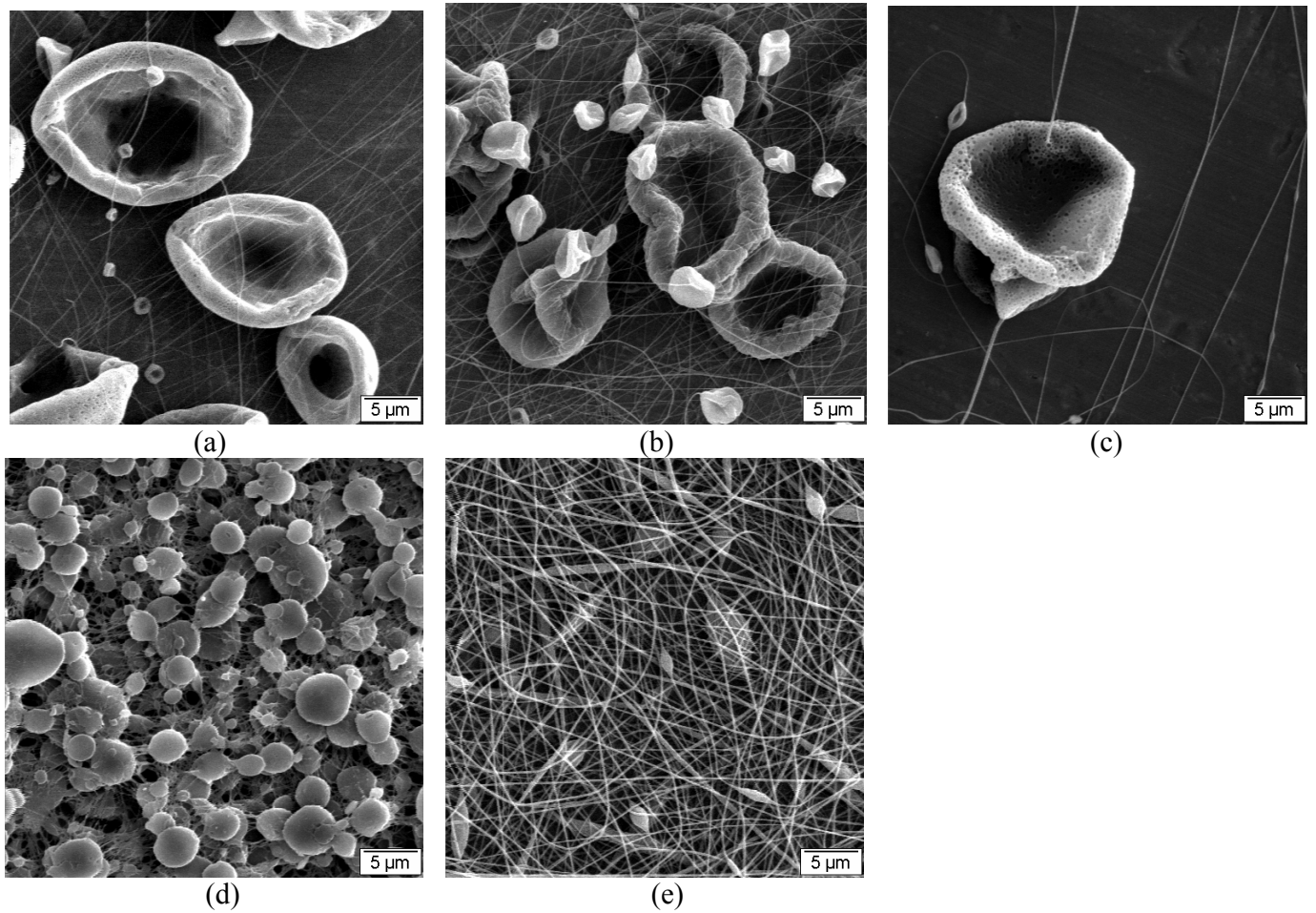

(a) (b) (c)

(d) (e)

Fig. 2. *SEM photographs of polystyrene fibers and beads electrospun with various solvents (a: THF, b: Chloroform, c: CS_2, d: NMP, e: DMF).*

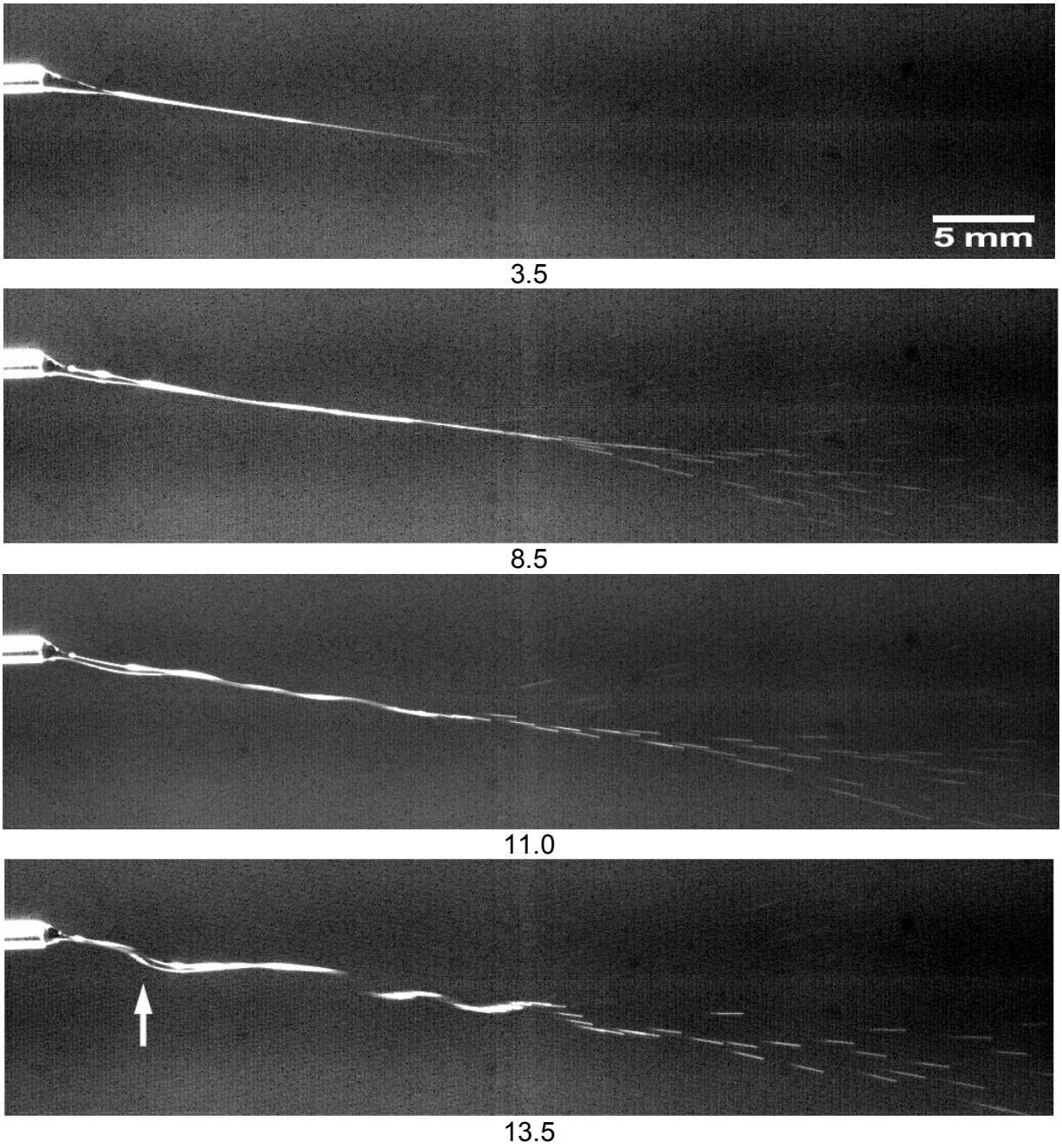

Fig. 3. *Sequential photographs showing the initial development of instabilities in the primary jet emerging from the capillary. The segment indicated by the arrow develops further jet instability shown in Fig. 4. The numbers indicate the time elapsed (ms) after the jet emerges from the Taylor cone. (Solvent: THF, C = 0.072 g/mL)*

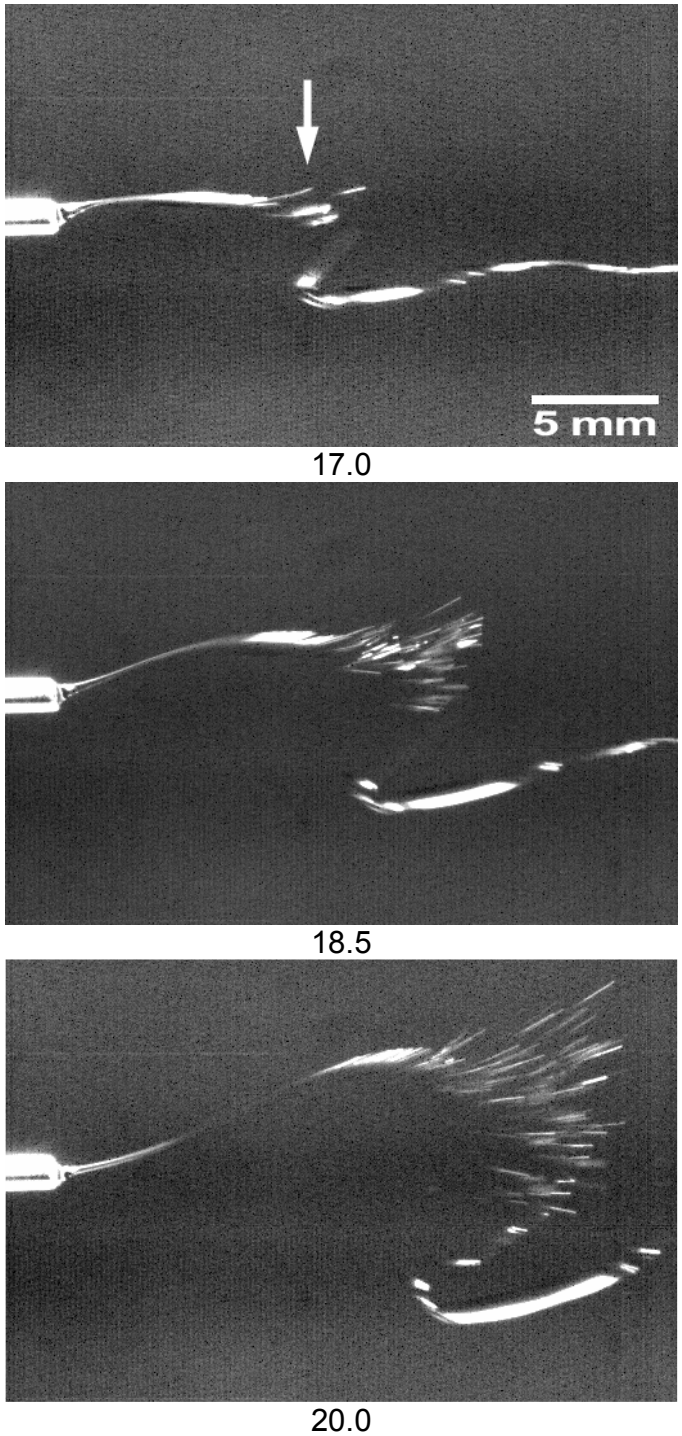

Fig. 4. *Images showing a growing perturbation leading to the breakup of the primary jet. The arrow indicates the loops created due to bending instability. The numbers indicate the time elapsed (ms) after the jet emerged from the Taylor cone. (Solvent: THF, C = 0.072 g/mL)*

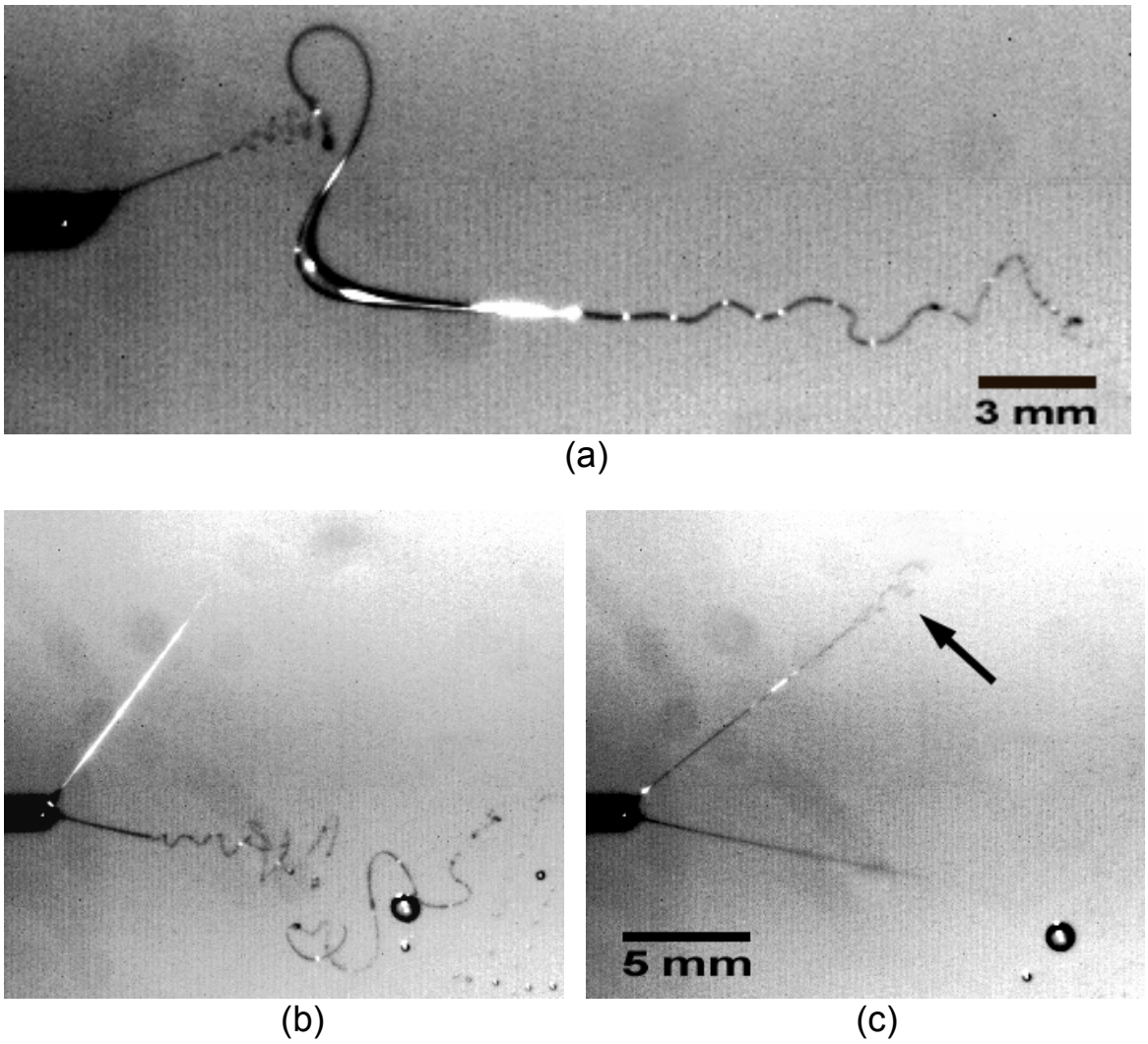

Fig. 5. *Photographs showing (a) the primary jet undergoing bending instability, (b) the development of a secondary jet and (c) bending instability in the secondary jet (indicated by the arrow). The time elapsed (after the primary jet emerges from the Taylor cone) for the formation of the secondary jet is typically on the order of 20 ms. (Solvent: THF, C = 0.078 g/mL)*

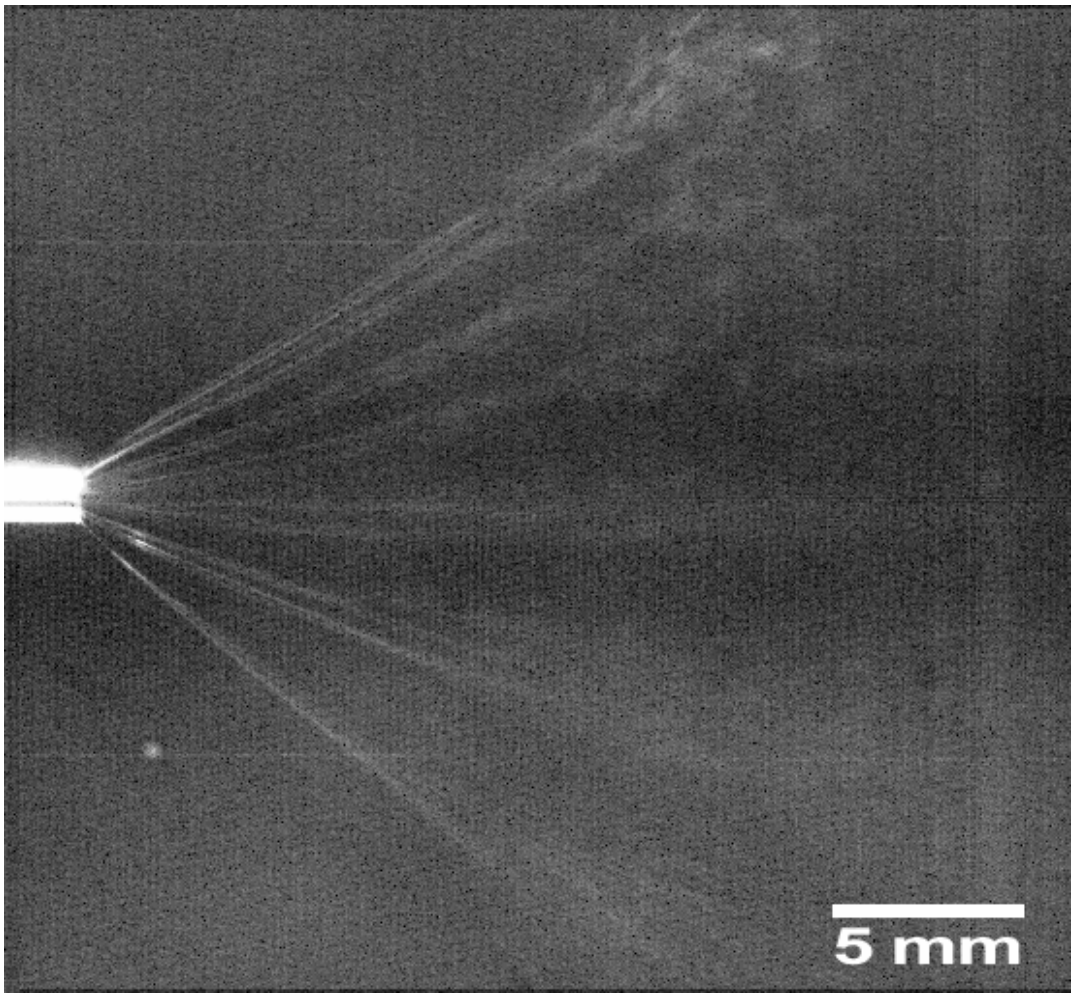

Fig. 6. *Photograph showing numerous minijets emerging from the capillary under steady-state conditions. The time elapsed after the initial jet emerged from the Taylor cone is 43.5 ms. (Solvent: THF, C = 0.072 g/mL)*

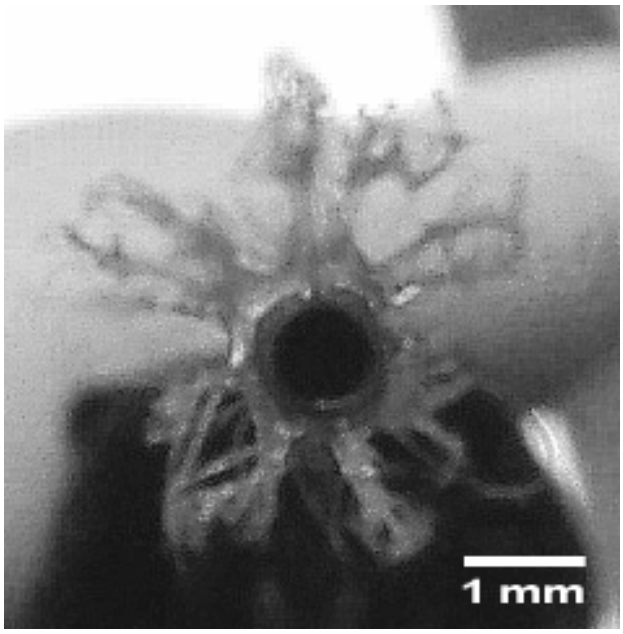

Fig. 7. *Photograph showing the tip of the needle at the end of the experiment. Numerous solidified fibers can be observed in the radial direction around the capillary edge. (Solvent: THF, C = 0.072 g/mL)*

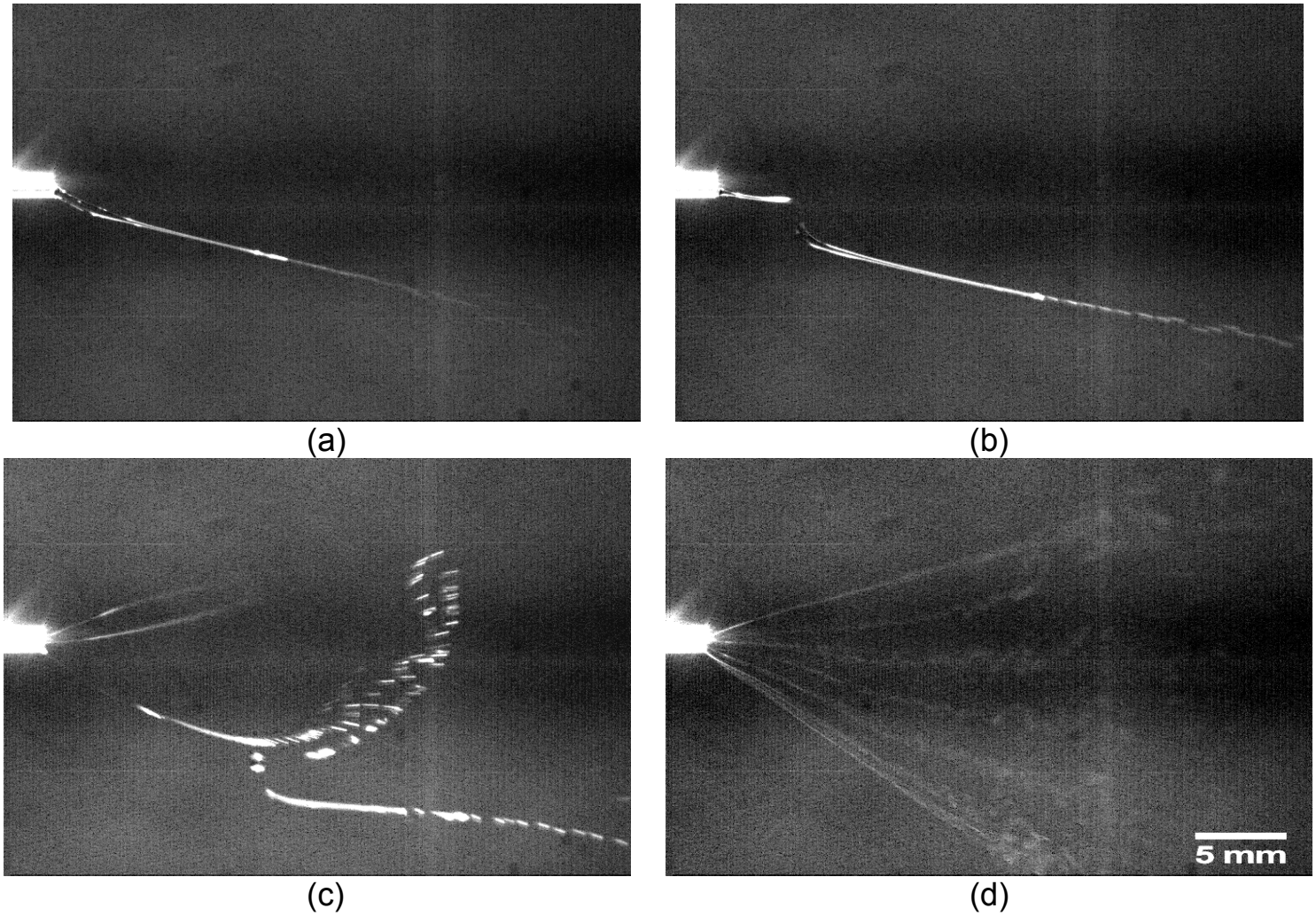

Fig. 8. *Photographs showing the jet development and breakdown during electrospinning with chloroform as the solvent: (a) elongational flow, (b) development of bending instability, (c) breakup of primary jet and emergence of secondary jets, and (d) numerous jets under steady state. (C = 0.070 g/mL)*

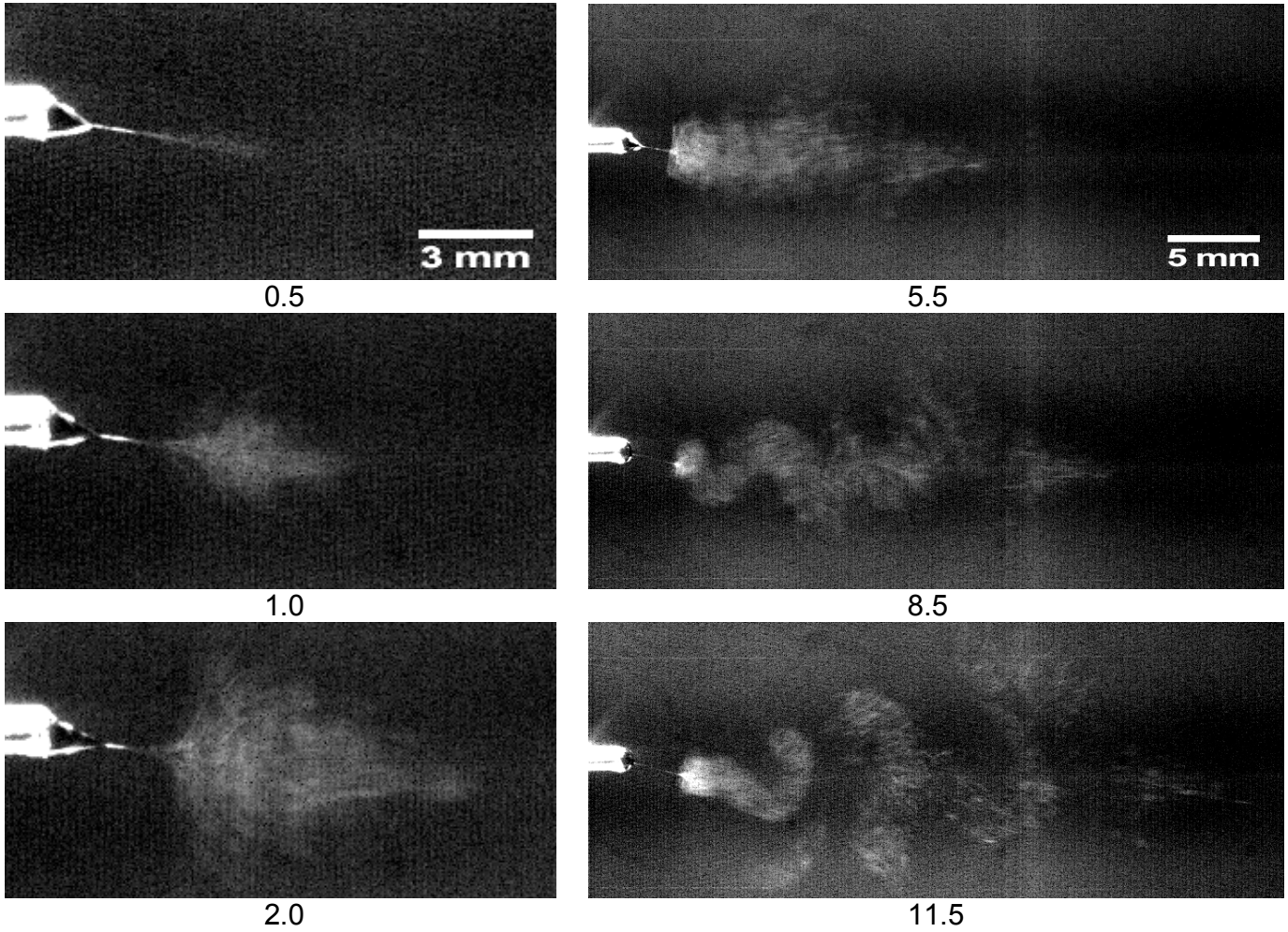

Fig. 9. *Sequential photographs showing morphological changes in the primary jet during electrospinning with DMF as the solvent. The numbers indicate the time elapsed (ms) after the jet emerged from the Taylor cone. Note the oscillations in the primary jet after 5.5 ms. (C = 0.120 g/mL)*

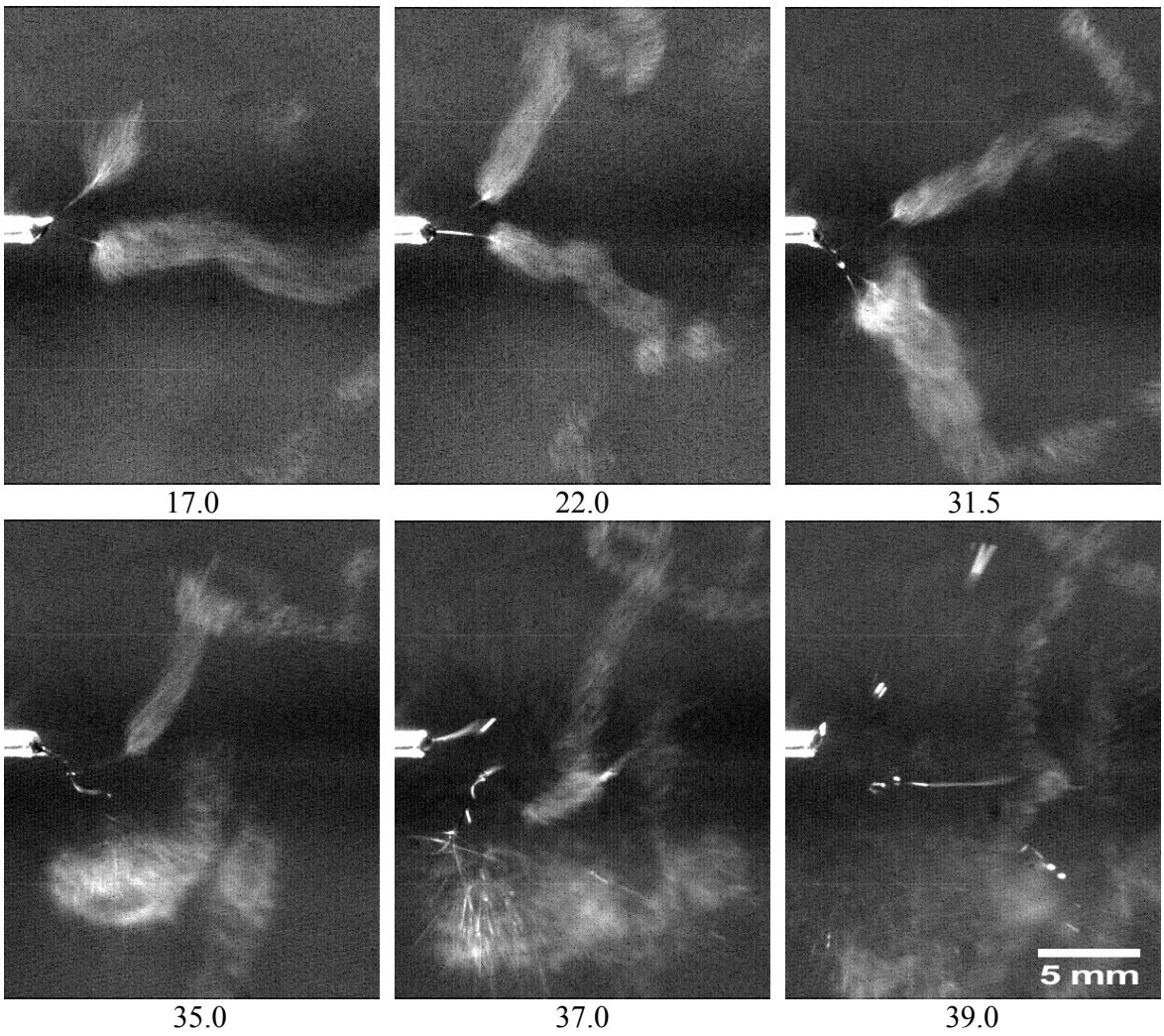

Fig. 10. *Photographs showing the development and breakdown of the secondary jet during electrospinning with DMF as the solvent. The numbers indicate the time elapsed (ms) after the jet emerges from the Taylor cone. Note the whipping instability that develops after 35.0 ms. (C = 0.120 g/mL)*

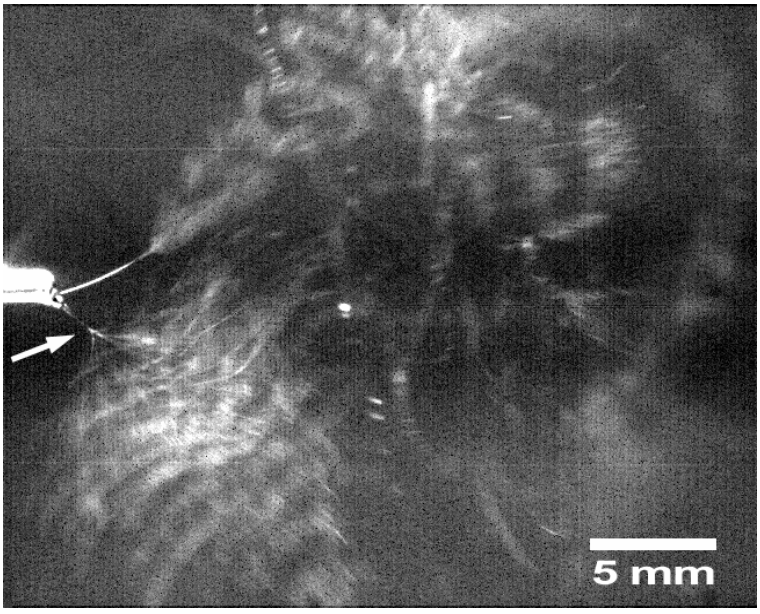

Fig. 11. *Photograph showing examples of extremely chaotic jets that undergo extensive splitting and whipping during electrospinning with DMF as the solvent. Such chaotic events are typically observed before a steady-state pattern develops. (C = 0.120 g/mL)*

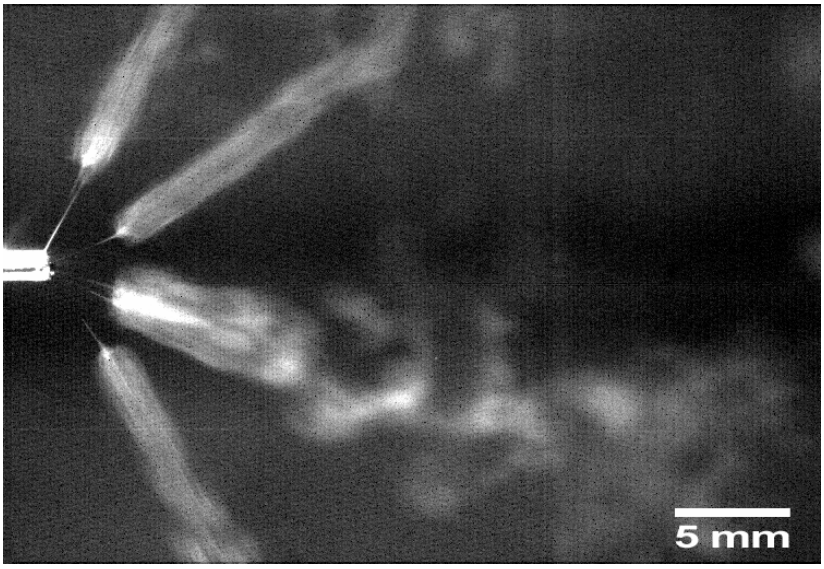

Fig. 12. *Photograph showing several jets emerging from the capillary under steady-state conditions during electrospinning with DMF as the solvent. The time elapsed after the initial jet emerged from the Taylor cone is 181.5 ms. (C= 0.120 g/mL)*

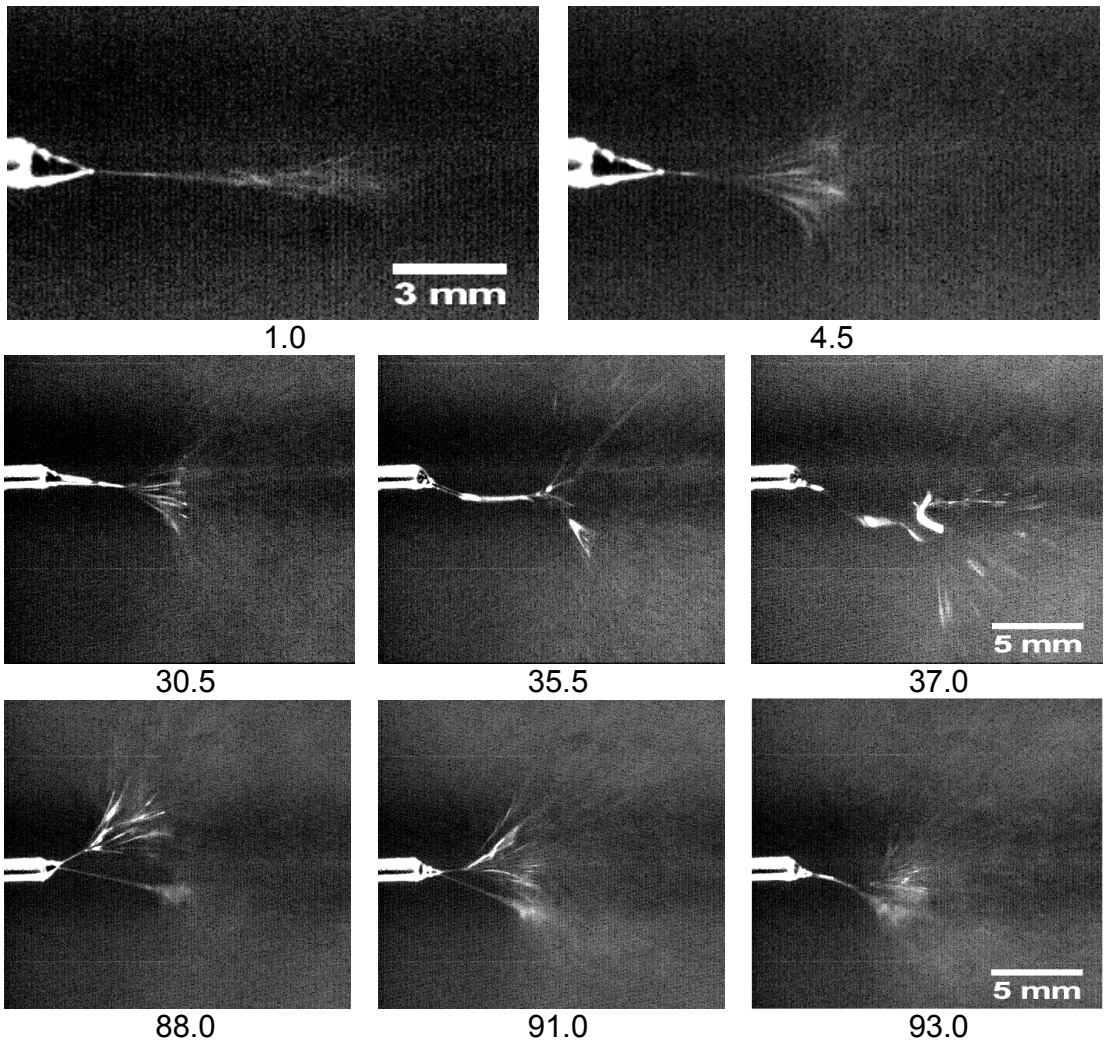

Fig. 13. *Photographs showing the jet breakdown during electrospinning with NMP as the solvent. The numbers indicate the time elapsed (ms) after the jet emerges from the Taylor cone. (C = 0.071 g/mL)*

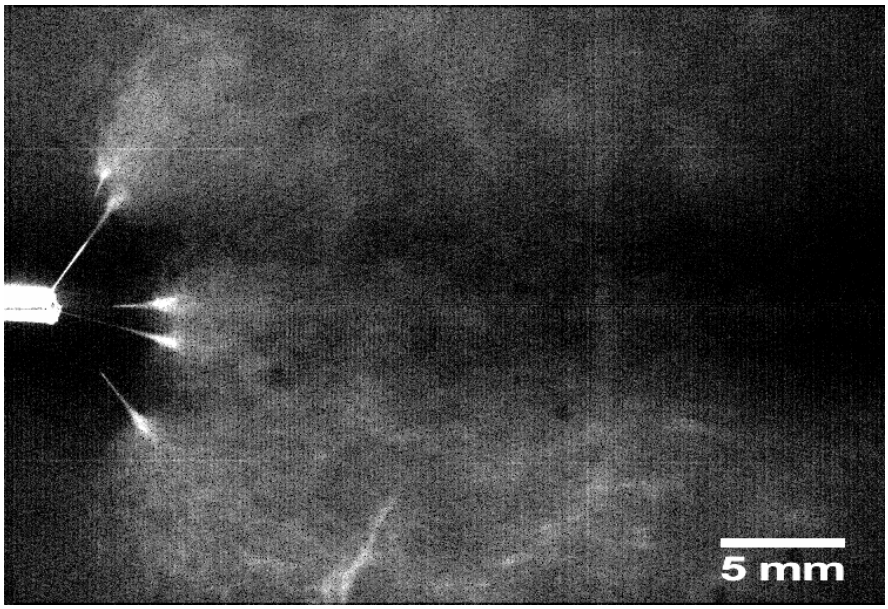

Fig. 14. *Photograph showing several jets emerging from the capillary under steady-state conditions during electrospinning with DMF as the solvent. The time elapsed after the initial jet emerged from the Taylor cone is 161 ms. (C = 0.071 g/mL)*

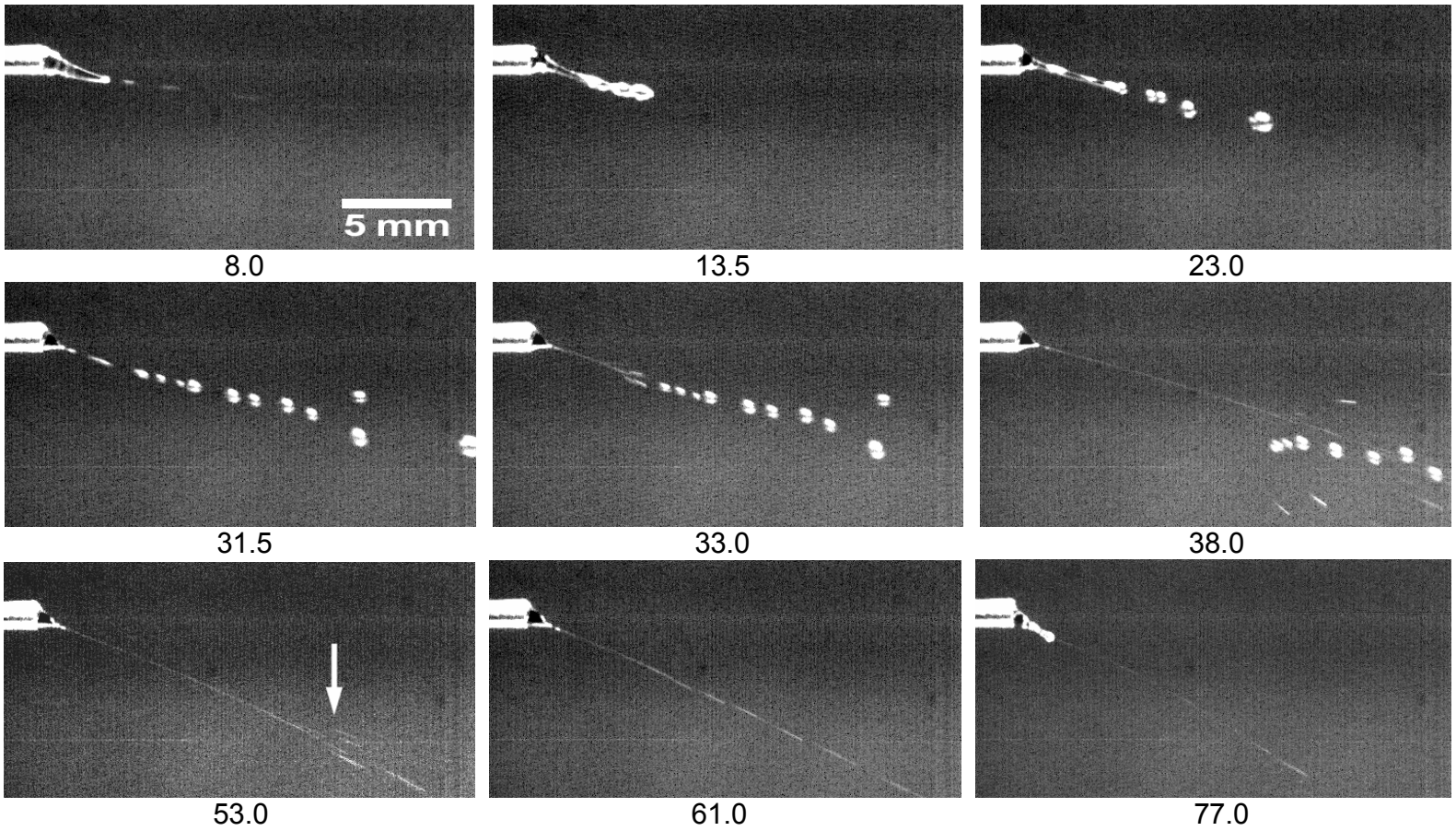

Fig. 15. *Photographs showing the jet breakdown during electrospinning with CS_2 as the solvent. The numbers indicate the time elapsed (ms) after the initial droplet emerges from the Taylor cone. The arrow indicates the breakup of a single steady state jet. (C = 0.072 g/mL)*

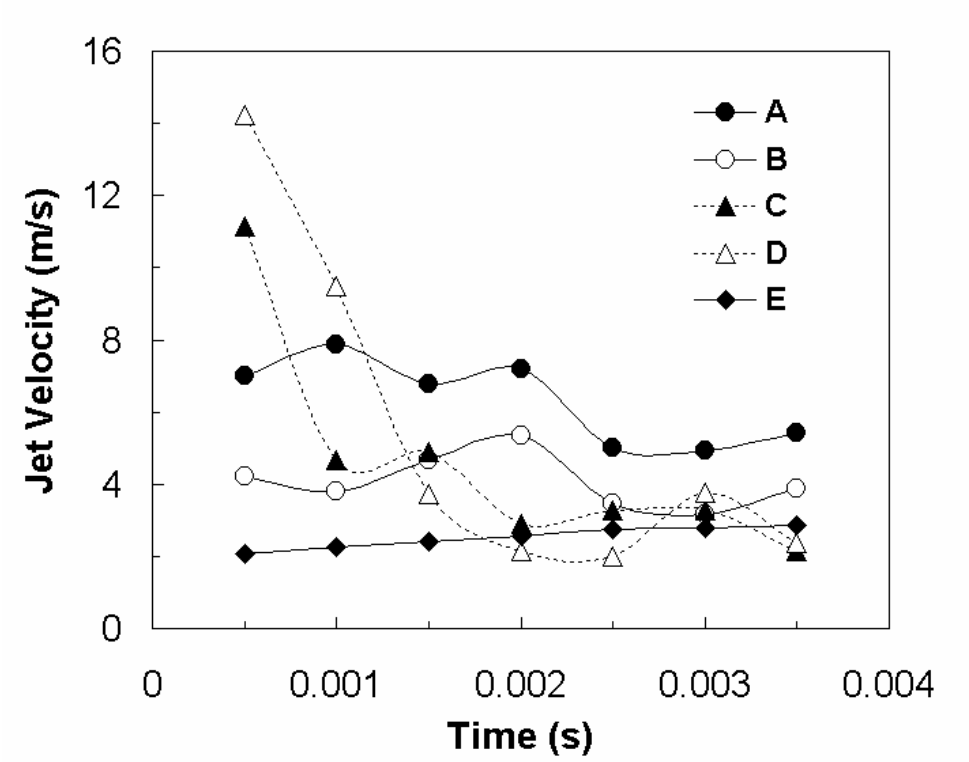

Fig. 16. *Jet velocity as a function of time for various solvents. The time was measured after a stable jet emerged from Taylor cone. The typical standard deviation was around ±2m/s. (A: THF, B: chloroform, C: DMF, D: NMP, E: CS_2)*

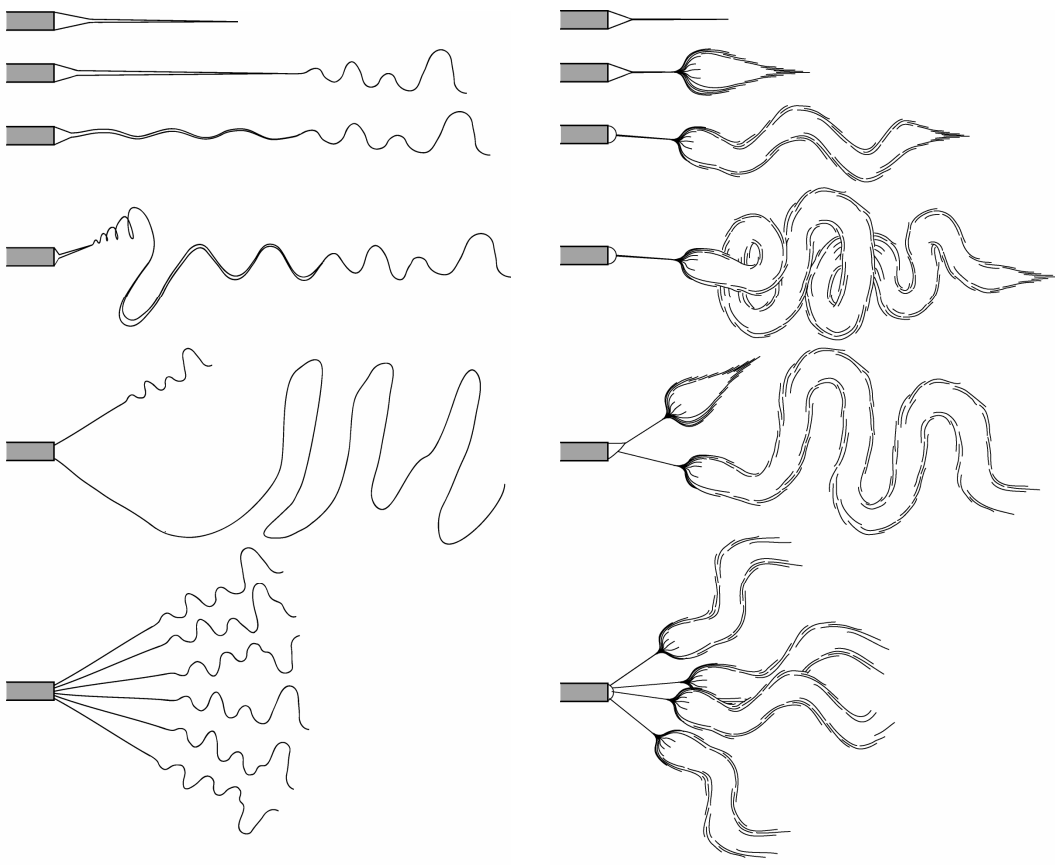

Fig. 17. Schematic of jet breakdown exhibited by two groups of solvent.

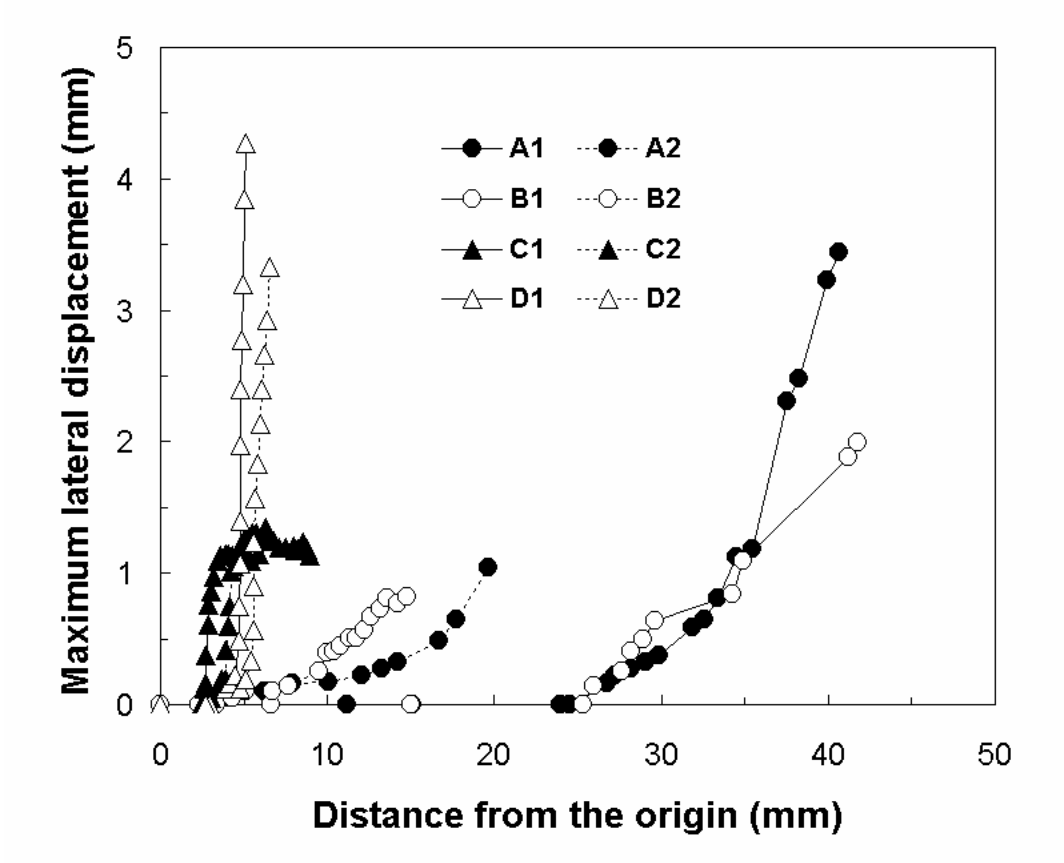

Fig. 18. *Maximum size of the envelope cone formed during jet instability measured from a photograph. (A: THF, B: chloroform, C: DMF, D: NMP) Numbers 1 and 2 indicate primary and secondary jet respectively.*